Table 3. Multivariate analysis to estimate the effect of lower body weight on TDF-associated renal dysfunction.

	Model 1 Crude		Model 2 Adjusted		Model 3 Adjusted	
	HR	95%CI	HR	95%CI	HR	95%CI
Weight per 5 kg decrement¶	1.23	1.10–1.37	1.21	1.07–1.36	1.13	1.01–1.27
Male gender			0.88	0.41–1.89	0.57	0.26–1.26
Age per 10 years¶			1.16	0.98–1.38	1.24	1.04–1.49
Serum creatinine >0.8 mg/dl					0.62	0.35–1.07
CD4 count <200/μl					1.65	0.97–2.79
HIV viral load per log10/ml					1.05	0.90–1.23
Boosted PIs					1.54	0.93–2.54
Concurrent use of nephrotoxic drug					1.23	0.77–1.97
Hepatitis C					1.57	0.92–2.69
Smoking¶					1.65	1.09–2.48

¶P<0.05 in Model 3.
TDF: tenofovir, HR: hazard ratio, CI: confidence interval, PI: protease inhibitor.
doi:10.1371/journal.pone.0022661.t003

>67 kg. Fourthly, the number (percentage) of patients whose eGFR decreased to <60 ml/min/1.73 m^2 was not different among the baseline weight categories (p = 0.229), whereas the number of patients who discontinued TDF with a clinical diagnosis of renal dysfunction due to TDF varied significantly according to body weight (p = 0.001, chi-square test, Table 6). None of the patients showed reduction of eGFR to <10 ml/min/1.73 m^2.

Discussion

In this Japanese cohort, 19.6% of the patients experienced eGFR decline of more than 25% from the baseline after commencement of TDF. The incidence of TDF-associated renal dysfunction was 10.5 per 100 person-years. Multivariate analysis identified smaller body weight and smaller body mass index as significant and almost significant factors, respectively, for TDF-associated renal dysfunction.

The incidence of TDF-associated renal dysfunction in patients with small body weight might be higher than previously reported in studies of patients with larger statures. Studies from North America, Europe, and Australia reported an incidence of <1% to 4.3% for TDF-related renal dysfunction, although the definition used for the diagnosis of renal impairment was different among the studies and varied from an increase in serum creatinine from >0.5 to >2 mg/dL from baseline [1–3,5,13]. Several studies conducted in these regions indicated that the range of patients' mean body weight was 69–74 kg, indicating that their patients were heavier than those of the present study with a median weight of 63 kg [2,6,12,14]. The impact of the comparatively lower body weight seems stronger in our patients probably because they do not appear to have many of the other established risk factors for TDF-associated renal dysfunction despite the high incidence of 10.5 per 100 person-years. For example, they were comparatively young with a median age of 38 years, CD4 count was relatively maintained, and approximately 30% had suppressed HIV viral load at baseline (Table 1). Furthermore, they were less likely to have hypertension, dyslipidemia, and diabetes mellitus.

Table 4. Multivariate analysis to estimate the impact of BMI decrement on TDF-associated renal dysfunction.

	Model 1 Crude		Model 2 Adjusted		Model 3 Adjusted	
	HR	95%CI	HR	95%CI	HR	95%CI
BMI per 1 kg/m^2 decrement	1.14	1.05–1.23	1.13	1.05–1.22	1.07	1.00–1.16
Male gender			0.67	0.32–1.38	0.48	0.23–1.03
Age per 10 years¶			1.20	1.01–1.43	1.27	1.06–1.52
Serum creatinine >0.8 mg/dl					0.60	0.35–1.04
CD4 count <200/μl					1.64	0.97–2.79
HIV viral load per log10/ml					1.05	0.90–1.23
Boosted PIs					1.49	0.90–2.45
Concurrent use of nephrotoxic drugs					1.22	0.76–1.94
Hepatitis C					1.62	0.94–2.76
Smoking¶					1.63	1.08–2.46

¶P<0.05 in Model 3.
BMI: body mass index, TDF: tenofovir, HR: hazard ratio, CI: confidence interval, PI: protease inhibitor.
doi:10.1371/journal.pone.0022661.t004

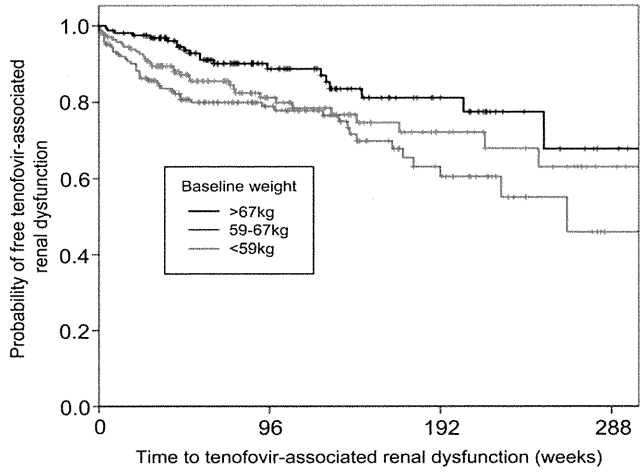

Figure 3. Kaplan-Meier curve showing the time to 25% reduction in eGFR according to baseline weight categories. Compared to patients with body weight >67 kg, those with weight <59 kg were more likely to develop >25% decline in eGFR (P = 0.002), whereas those with weight 59–67 kg showed only a marginal significance (P = 0.073, log-rank test). eGFR: estimated glomerular filtration rate.
doi:10.1371/journal.pone.0022661.g003

The results of multivariate analysis that each 5 kg decrement in body weight was significantly associated with TDF-associated renal dysfunction but not each 1 kg/m^2 decrement in BMI suggests that weight might be more useful and handy information to estimate the risk for TDF-associated renal dysfunction than BMI. Thus, patient's body weight is an important risk factor to consider at the time of TDF prescription.

Our study is one of a few that have examined the impact of TDF-associated renal dysfunction in patients with small body weight, but is the first to examine the impact of small body weight as a primary exposure by creating the model used for multivariate analysis [16–18]. One study from Thailand that included patients with a median weight of 56.5 kg reported a similar incidence of 16.2 per 100 person-years for developing TDF-associated renal dysfunction [17]. They concluded that the small body weight of their patients was probably associated with the high incidence of TDF-associated renal dysfunction. Our study confirmed that conclusion and provided statistically-backed evidence that small body weight is a significant risk factor of TDF-associated renal dysfunction by using a multivariate model with least multi-collinearity to evaluate the impact of small body weight. The results of the present study could be applied to many countries in Asia and Africa, where stature and body weight of the population are comparatively smaller.

This study adopted a decrease in eGFR of >25% as a definition for TDF-associated renal dysfunction. This criterion is one of common methods in evaluating renal function [22,23]. Using this definition, however, does not mean that all patients with >25% fall in eGFR have severe renal dysfunction. However, the definition of renal dysfunction based on a fall in eGFR of >25% is probably more sensitive than that based on eGFR <60 ml/min/1.73 m^2, in patients with comparatively good baseline renal function, such as patients of our study. Adopting this definition could be useful in detecting early renal dysfunction and in the clinical decision making regarding the need for certain interventions, for example, discontinuation of TDF. Early detection of renal dysfunction is particularly important in patients with HIV infection, because kidney disease may be associated with AIDS and death, and TDF-associated renal dysfunction might be irreversible [27,28].

Since the calculation of eGFR using the MDRD formula is based on serum creatinine, age, race and gender, any fall in eGFR is influenced by hypercreatininemia caused by increased muscle mass [29]. It is possible that the muscle mass increases in patients on ART, especially those with low weight at baseline compared to those with higher weight, reflecting reversal of wasting in those patients who were most malnourished. Such increase in muscle mass could then result in a fall in eGFR despite no change in actual renal elimination of creatinine. However, complementary analysis showed that weight change throughout the follow-up period was not significantly different among patients with different baseline weight, and the sensitivity analysis demonstrated that weight change did not alter the significance of every 5 kg decrement.

In the present study, high eGFR and low serum creatinine levels at baseline were identified as risk factors for falls in eGFR of more than 25%, in contrast to several previous studies that showed high serum creatinine and low eGFR were risk factors [4,10,25]. While the exact reason for this discrepancy is unknown at present, it could be related to differences in the definition of TDF-associated renal dysfunction. The aforementioned Thai study used the same definition applied in the present study and a Canadian study that used the definition of 1.5-fold increase in serum creatinine from baseline also reported high eGFR and low serum creatinine level at baseline as risk factors [17,30]. Thus, it is plausible to observe a fall in eGFR when the baseline value is high, since Horberg et al. reported that patients with baseline eGFR of >80 ml/min/1.73 m^2 were likely to show a pronounced fall in eGFR with TDF use [31].

Multivariate analysis also suggested that old age and current smoking are significant risks for TDF-associated renal dysfunction

Table 5. Median and interquartile range of the actual fall in eGFR from the baseline to 24, 48, and 96 weeks, according to body weight.

	Total (n = 495)		<59 kg (n = 167)		59–67 kg (n = 168)		>67 kg (n = 160)	
	fall in eGFR(ml/min/1.73 m^2)		fall in eGFR		fall in eGFR		fall in eGFR	
	median	IQR	median	IQR	median	IQR	median	IQR
to 24 weeks	7.8	(−1.7–18.1)	9.8	(−3.6–22.6)	6.8	(−1.5–17.3)	7.3	(−1.8–15.4)
to 48 weeks	9.0	(−0.7–21.9)	13.0	(−0.2–29.3)	7.2	(−1.2–20.0)	8.1	(−0.6–18.6)
to 96 weeks	9.3	(−0.5–23.1)	13.4	(1.2–33.2)	8.6	(−0.2–21.7)	7.5	(−2.4–19.8)

eGFR: estimated glomerular filtration rate, IQR: interquartile range.
doi:10.1371/journal.pone.0022661.t005

Table 6. Number of patients whose eGFR decreased to <60 ml/min/1.73 m^2 and who discontinued tenofovir with clinical diagnosis of renal dysfunction due to tenofovir.

	<59 kg (n = 167)	59–67 kg (n = 168)	>67 kg (n = 160)	p value
eGFR <60 ml/min/1.73 m^2	4 (2.4%)	1 (0.6%)	1 (0.6%)	0.229
Discontinued tenofovir	16 (9.6%)	8 (4.8%)	1 (0.6%)	0.001
Reasons for discontinuation				
>25% eGFR decrement	8 (4.8%)	4 (2.4%)	0 (0%)	
Urine β2 microglobulin >5000 μg/l	11 (6.6%)	4 (2.4%)	1 (0.6%)	

Among the patients who discontinued tenofovir, both >25% fall in eGFR and urine β2 microglobulin >5000 μg/l were registered in six patients with body weight <59 kg, and in three patients with body weight 59–67 kg.
eGFR: estimated glomerular filtration rate.
doi:10.1371/journal.pone.0022661.t006

(Table 3, Model 3 and Table 4, Model 3). However, these results have to be interpreted with caution, because these multivariate analyses were formulated to primarily evaluate weight decrement, not age or smoking.

The mechanism of TDF-associated renal dysfunction is not fully understood. TDF-associated renal dysfunction probably develops as a result of complex interaction of pharmacological, environmental, and genetic factors, rather than small body weight only [32]. It should be noted, however, that small body weight has been identified as a risk factor for TDF-associated renal dysfunction not only in clinical trials, but also in *in vitro* and pharmacokinetic studies [33–36]. TDF is the prodrug of acyclic nucleotide analog tenofovir, which is excreted by both glomerular filtration and active tubular secretion. *In vitro* studies showed that tenofovir exhibits mitochondrial toxicity in renal proximal tubular cells, and animal studies demonstrated that renal tubular dysfunction was associated with the dose and plasma drug concentrations of TDF [34,35]. Furthermore, pharmacokinetic studies showed that small body weight is associated with reduced plasma TDF clearance and thus high plasma TDF concentrations, which could result in renal tubular dysfunction. [33,36].

There are several limitations to our study. First, because of the retrospective nature of the study, patients with possible risks for TDF-associated renal dysfunction could have not been prescribed TDF. Because of this selection bias, the incidence of TDF-associated renal dysfunction might be underestimated. Second, the study did not compare the incidence of renal dysfunction in a control group (TDF-free ART). Due to the small body weight in Japanese or other factors such as genetics, the use of ART without TDF might cause higher incidence of renal dysfunction as well. Third, as discussed above, the definition of TDF-associated renal dysfunction, especially the criteria used to evaluate proximal renal tubular damage, is not uniformly established in the field and is different in the published studies. Accordingly, we decided to adopt changes in eGFR, instead of parameters for proximal renal tubular damage. Using the eGFR as a marker for TDF-associated renal dysfunction, our results might have underestimated the incidence of TDF-associated renal dysfunction.

In conclusion, the present study demonstrated a high incidence of TDF-associated renal dysfunction among Japanese patients, a potentially high-risk group due to the low median body weight. The results also identified small body weight as a risk for TDF-associated renal dysfunction in a statistical model that included small body weight as a primary exposure. TDF is certainly a drug of choice for one of the components of the first line therapies for HIV infection. However, the importance of close monitoring for renal function in patients with small body weight should be emphasized for early detection of TDF-associated renal dysfunction.

Supporting Information

Text S1 Letter of Approval from Human Research Ethics Committee of National Center for Global Health and Medicine.
(PDF)

Dataset S1 Raw data of the target population.
(XLS)

Acknowledgments

The authors thank all the clinical staff at the AIDS Clinical Center for their help in completion of this study.

Author Contributions

Conceived and designed the experiments: AN TH KU TN MKS. Performed the experiments: AN H. Sakai. Analyzed the data: AN TH KU KO IK H. Sakai. TN MKS. Contributed reagents/materials/analysis tools: H. Suemori H. Sakai. Wrote the manuscript: AN TN MKS.

References

1. Gallant JE, DeJesus E, Arribas JR, Pozniak AL, Gazzard B, et al. (2006) Tenofovir DF, emtricitabine, and efavirenz vs. zidovudine, lamivudine, and efavirenz for HIV. N Engl J Med 354: 251–260.
2. Gallant JE, Staszewski S, Pozniak AL, DeJesus E, Suleiman JM, et al. (2004) Efficacy and safety of tenofovir DF vs stavudine in combination therapy in antiretroviral-naive patients: a 3-year randomized trial. JAMA 292: 191–201.
3. Izzedine H, Hulot JS, Vittecoq D, Gallant JE, Staszewski S, et al. (2005) Long-term renal safety of tenofovir disoproxil fumarate in antiretroviral-naive HIV-1-infected patients. Data from a double-blind randomized active-controlled multicentre study. Nephrol Dial Transplant 20: 743–746.
4. Nelson MR, Katlama C, Montaner JS, Cooper DA, Gazzard B, et al. (2007) The safety of tenofovir disoproxil fumarate for the treatment of HIV infection in adults: the first 4 years. AIDS 21: 1273–1281.
5. Arribas JR, Pozniak AL, Gallant JE, Dejesus E, Gazzard B, et al. (2008) Tenofovir disoproxil fumarate, emtricitabine, and efavirenz compared with zidovudine/lamivudine and efavirenz in treatment-naive patients: 144-week analysis. J Acquir Immune Defic Syndr 47: 74–78.
6. Post FA, Moyle GJ, Stellbrink HJ, Domingo P, Podzamczer D, et al. (2010) Randomized comparison of renal effects, efficacy, and safety with once-daily abacavir/lamivudine versus tenofovir/emtricitabine, administered with efavir-

enz, in antiretroviral-naive, HIV-1-infected adults: 48-week results from the ASSERT study. J Acquir Immune Defic Syndr 55: 49–57.
7. Verhelst D, Monge M, Meynard JL, Fouqueray B, Mougenot B, et al. (2002) Fanconi syndrome and renal failure induced by tenofovir: a first case report. Am J Kidney Dis 40: 1331–1333.
8. Schaaf B, Aries SP, Kramme E, Steinhoff J, Dalhoff K (2003) Acute renal failure associated with tenofovir treatment in a patient with acquired immunodeficiency syndrome. Clin Infect Dis 37: e41–43.
9. Rollot F, Nazal EM, Chauvelot-Moachon L, Kelaidi C, Daniel N, et al. (2003) Tenofovir-related Fanconi syndrome with nephrogenic diabetes insipidus in a patient with acquired immunodeficiency syndrome: the role of lopinavir-ritonavir-didanosine. Clin Infect Dis 37: e174–176.
10. Peyriere H, Reynes J, Rouanet I, Daniel N, de Boever CM, et al. (2004) Renal tubular dysfunction associated with tenofovir therapy: report of 7 cases. J Acquir Immune Defic Syndr 35: 269–273.
11. Kinai E, Hanabusa H (2009) Progressive renal tubular dysfunction associated with long-term use of tenofovir DF. AIDS Res Hum Retroviruses 25: 387–394.
12. Winston A, Amin J, Mallon P, Marriott D, Carr A, et al. (2006) Minor changes in calculated creatinine clearance and anion-gap are associated with tenofovir disoproxil fumarate-containing highly active antiretroviral therapy. HIV Med 7: 105–111.
13. Gallant JE, Winston JA, DeJesus E, Pozniak AL, Chen SS, et al. (2008) The 3-year renal safety of a tenofovir disoproxil fumarate vs. a thymidine analogue-containing regimen in antiretroviral-naive patients. AIDS 22: 2155–2163.
14. Fux CA, Simcock M, Wolbers M, Bucher HC, Hirschel B, et al. (2007) Tenofovir use is associated with a reduction in calculated glomerular filtration rates in the Swiss HIV Cohort Study. Antivir Ther 12: 1165–1173.
15. Cooper RD, Wiebe N, Smith N, Keiser P, Naicker S, et al. (2010) Systematic review and meta-analysis: renal safety of tenofovir disoproxil fumarate in HIV-infected patients. Clin Infect Dis 51: 496–505.
16. Gayet-Ageron A, Ananworanich J, Jupimai T, Chetchotisakd P, Prasithsirikul W, et al. (2007) No change in calculated creatinine clearance after tenofovir initiation among Thai patients. J Antimicrob Chemother 59: 1034–1037.
17. Chaisiri K, Bowonwatanuwong C, Kasettratat N, Kiertiburanakul S (2010) Incidence and risk factors for tenofovir-associated renal function decline among Thai HIV-infected patients with low-body weight. Curr HIV Res 8: 504–509.
18. Reid A, Stohr W, Walker AS, Williams IG, Kityo C, et al. (2008) Severe renal dysfunction and risk factors associated with renal impairment in HIV-infected adults in Africa initiating antiretroviral therapy. Clin Infect Dis 46: 1271–1281.
19. Gatanaga H, Tachikawa N, Kikuchi Y, Teruya K, Genka I, et al. (2006) Urinary beta2-microglobulin as a possible sensitive marker for renal injury caused by tenofovir disoproxil fumarate. AIDS Res Hum Retroviruses 22: 744–748.
20. Goicoechea M, Liu S, Best B, Sun S, Jain S, et al. (2008) Greater tenofovir-associated renal function decline with protease inhibitor-based versus nonnucleoside reverse-transcriptase inhibitor-based therapy. J Infect Dis 197: 102–108.
21. Rodriguez-Novoa S, Labarga P, Soriano V, Egan D, Albalater M, et al. (2009) Predictors of kidney tubular dysfunction in HIV-infected patients treated with tenofovir: a pharmacogenetic study. Clin Infect Dis 48: e108–116.
22. Bash LD, Coresh J, Kottgen A, Parekh RS, Fulop T, et al. (2009) Defining incident chronic kidney disease in the research setting: The ARIC Study. Am J Epidemiol 170: 414–424.
23. Chue CD, Edwards NC, Davis LJ, Steeds RP, Townend JN, et al. (2011) Serum phosphate but not pulse wave velocity predicts decline in renal function in patients with early chronic kidney disease. Nephrol Dial Transplant;doi: 10.1093/ndt/gfq78.
24. Levey AS, Coresh J, Greene T, Stevens LA, Zhang YL, et al. (2006) Using standardized serum creatinine values in the modification of diet in renal disease study equation for estimating glomerular filtration rate. Ann Intern Med 145: 247–254.
25. Gupta SK, Eustace JA, Winston JA, Boydstun II, Ahuja TS, et al. (2005) Guidelines for the management of chronic kidney disease in HIV-infected patients: recommendations of the HIV Medicine Association of the Infectious Diseases Society of America. Clin Infect Dis 40: 1559–1585.
26. Lomaestro BM (2000) Fluoroquinolone-induced renal failure. Drug Saf 22: 479–485.
27. Wever K, van Agtmael MA, Carr A (2010) Incomplete reversibility of tenofovir-related renal toxicity in HIV-infected men. J Acquir Immune Defic Syndr 55: 78–81.
28. Szczech LA, Hoover DR, Feldman JG, Cohen MH, Gange SJ, et al. (2004) Association between renal disease and outcomes among HIV-infected women receiving or not receiving antiretroviral therapy. Clin Infect Dis 39: 1199–1206.
29. Baxmann AC, Ahmed MS, Marques NC, Menon VB, Pereira AB, et al. (2008) Influence of muscle mass and physical activity on serum and urinary creatinine and serum cystatin C. Clin J Am Soc Nephrol 3: 348–354.
30. Antoniou T, Raboud J, Chirhin S, Yoong D, Govan V, et al. (2005) Incidence of and risk factors for tenofovir-induced nephrotoxicity: a retrospective cohort study. HIV Med 6: 284–290.
31. Horberg M, Tang B, Towner W, Silverberg M, Bersoff-Matcha S, et al. (2010) Impact of tenofovir on renal function in HIV-infected, antiretroviral-naive patients. J Acquir Immune Defic Syndr 53: 62–69.
32. Post FA, Holt SG (2009) Recent developments in HIV and the kidney. Curr Opin Infect Dis 22: 43–48.
33. Jullien V, Treluyer JM, Rey E, Jaffray P, Krivine A, et al. (2005) Population pharmacokinetics of tenofovir in human immunodeficiency virus-infected patients taking highly active antiretroviral therapy. Antimicrob Agents Chemother 49: 3361–3366.
34. Van Rompay KK, Durand-Gasselin L, Brignolo LL, Ray AS, Abel K, et al. (2008) Chronic administration of tenofovir to rhesus macaques from infancy through adulthood and pregnancy: summary of pharmacokinetics and biological and virological effects. Antimicrob Agents Chemother 52: 3144–3160.
35. Kohler JJ, Hosseini SH, Hoying-Brandt A, Green E, Johnson DM, et al. (2009) Tenofovir renal toxicity targets mitochondria of renal proximal tubules. Lab Invest 89: 513–519.
36. Kiser JJ, Fletcher CV, Flynn PM, Cunningham CK, Wilson CM, et al. (2008) Pharmacokinetics of antiretroviral regimens containing tenofovir disoproxil fumarate and atazanavir-ritonavir in adolescents and young adults with human immunodeficiency virus infection. Antimicrob Agents Chemother 52: 631–637.

INTERNAL MEDICINE

□ ORIGINAL ARTICLE □

Clinical Symptoms and Courses of Primary HIV-1 Infection in Recent Years in Japan

Hideta Nakamura, Katsuji Teruya, Misao Takano, Kunihisa Tsukada, Junko Tanuma, Hirohisa Yazaki, Haruhito Honda, Miwako Honda, Hiroyuki Gatanaga, Yoshimi Kikuchi and Shinichi Oka

Abstract

Background The natural course of HIV-1 infection includes 10 years of an asymptomatic period before the development of AIDS. However, in Japan, the disease progression process seems faster in recent years.

Methods The study subjects were 108 new patients with primary HIV-1 infection during the period from 1997 through 2007. We evaluated their clinical symptoms and laboratory data, and then analyzed disease progression in 82 eligible patients. Disease progression was defined as a fall in CD4 count below 350/μL and/or initiation of antiretroviral therapy.

Results Ninety percent of the patients were infected via homosexual intercourse. All patients had at least one clinical symptom (mean; 4.75±1.99) related to primary HIV-1 infection, with a mean duration of 23.2 days (±14.8) and 53.3% of them had to be hospitalized due to severe symptoms. The mean CD4 count and viral load at first visit were 390/μL (±220.1) and 4.81 log10/mL (±0.78), respectively. None developed AIDS during the study period. Estimates of risk of disease progression were 61.0% at 48 weeks and 82.2% at 144 weeks. In patients who required antiretroviral therapy, the median CD4 count was 215/μL (range, 52-858) at initiation of such therapy. Among the patients with a CD4 count of <350/μL at first visit, 53% never showed recovery of CD4 count (>350/μL) without antiretroviral therapy.

Conclusion Despite possible bias in patient population, disease progression seemed faster in symptomatic Japanese patients with recently acquired primary HIV-1 infection than the previously defined natural course of the disease.

Key words: HIV-1, primary infection, disease progression

(Intern Med 50: 95-101, 2011)
(DOI: 10.2169/internalmedicine.50.4137)

Introduction

The natural course of HIV-1 infection has been well described in large cohorts from the United States and Europe before the introduction of highly active antiretroviral therapy (HAART); primary HIV-1 infection (PHI) is followed by a clinical latency, usually lasting around 10 years, which precedes the eventual collapse of the immune system (1, 2). However, there is a common feeling among clinicians at present that the natural disease progression of recently infected patients is faster than in previous years (3, 4). Disease progression depends on various factors such as HLA type (5), concomitant infections (6, 7), and available medical resources (8). In addition to these factors, events occurring during PHI could also determine the natural course of the disease. Initial studies suggested that patients with more symptoms related to primary PHI and longer duration of illness exhibit faster rates of progression to AIDS (9-13). Plasma viral load at a set point is also an independent predictor of disease progression (14, 15). However, to determine the viral set point is sometimes difficult. Therefore, for clinicians, the severity of clinical symptoms is the only predictor of subsequent disease progression. The latency be-

AIDS Clinical Center, National Center for Global Health and Medicine, Japan
Received for publication June 28, 2010; Accepted for publication September 29, 2010
Correspondence to Dr. Shinichi Oka, oka@acc.ncgm.go.jp

tween the development of PHI and commencement of HAART is also important in the present HAART era.

The main aim of this study was to evaluate the natural disease progression of recently infected Japanese patients. To determine whether or not the disease progression of recently infected patients is accelerated, their CD4 decline was compared with that of hemophiliacs infected before 1985 as the first HIV-1 infection in Japanese.

Furthermore, we also evaluated the correlation between initial CD4 count, viral load, and clinical events and subsequent changes in CD4 and/or time to start HAART in symptomatic Japanese patients with PHI.

Patients and Methods

Study site and patients with PHI

This study was conducted at the AIDS Clinical Center (ACC), National Center for Global Health and Medicine (NCGM: formerly International Medical Center of Japan). The NCGM (925 beds) is a tertiary general hospital located in central Tokyo and the ACC is the main referral clinic for treatment of HIV infected patients in Japan. As part of the follow-up service, HIV-1 infected patients usually visit the ACC on a monthly basis and CD4 count and viral load are measured at each visit. In the present retrospective study, we reviewed the medical records of 108 patients with PHI who were newly diagnosed with PHI between 1997 through 2007 at the ACC. We had conducted a clinical trial of structured treatment interruptions in patients with PHI from November 2000 through December 2002 and 26 patients were enrolled in that trial (16, 17). In terms of the data of these 26 patients, only the initial clinical and laboratory data were included in the present analysis, while all other data, such as time to events, were excluded from this study. To compare the natural CD4 decline of previously and recently infected patients, CD4 counts of 42 Japanese hemophiliacs recorded in the database in 1988 were analyzed as a previous control. Japanese hemophiliacs were infected with HIV-1 through contaminated blood products before 1985 (the estimated mean year of infection was 1983). Therefore, CD4 counts at the end of 1988 were the data at least 3 years after infection. In this comparison, the number of eligible recently infected patients was 59 patients; untreated and CD4 count at 3 years after infection was available.

Definition of PHI

PHI was diagnosed based on the presence of the following three criteria: 1) negative or incomplete western blot finding at the first visit with subsequent change to positive, 2) negative or weakly reactive enzyme-linked immunosorbent assay (ELISA) result for plasma HIV-1 RNA, and 3) confirmed HIV-1 infection on the first visit with documentation of negative ELISA result within 6 months. Symptomatic PHI was defined as PHI accompanied by at least one symptom related to acute retroviral syndrome, such as fever, lymphadenopathy, or skin rash.

Definition of disease progression

Disease progression was defined as fall in CD4 count below 350/μL and/or initiation of antiretroviral therapy. Specifically, patients with an AIDS-defined illness [listed under Centers for Disease Control and Prevention (CDC) category C], patients with AIDS requiring initiation of HAART, and those with severe symptomatic PHI on HAART were defined to have disease progression. The selection of a cutoff value of 350/μL for CD4 count was based on the fact that treatment is generally indicated during the chronic phase of infection when CD4 count falls below 350/μL (18). Patients were considered to be in immunologic progression at the first visit when the initial CD4 count was <350/μL and never subsequently reached 350/μL. For patients who showed a spontaneous increase in subsequent CD4 counts to ≥350/μL (such recovery occurred within 3 months from the first visit in all such patients), disease progression was set to have started at the time when such change in CD4 count occurred.

Statistical analysis

Continuous variables are presented as mean value ± SD. Categorical variables were presented as absolute numbers and proportions. Time to events was analyzed by the Kaplan-Meier survival curves, and compared using log-rank test. For patients who did not experience the events described above, data were censored at their last visit. To evaluate the differences between patients groups, the Student t test and χ^2 test were used when appropriate. The relationships between variables were analyzed by the Spearman rank-over correlation test. Statistical significance was defined as $p<0.05$. Data were analyzed using SPSS for Windows (version 15, SPSS, Inc., Chicago, IL).

Results

Table 1 lists the demographics of the enrolled patients with PHI. All patients had at least one documented symptom consistent with PHI (median 5; range 1-11). Fever, cervical lymphadenopathy, pharyngitis, and rash were found in more than 50% of patients (Table 2). The mean duration of symptoms was 23.2 days (SD ±14.8). Fifty-eight (53.7%) patients had to be hospitalized due to severe clinical symptoms. The initial viral loads in hospitalized patients were significantly higher than those of non-hospitalized patients. A longer duration of symptoms was associated with higher initial viral load (R=0.31, p=0.002) (Fig. 1A), and lower CD 4 count (R=-0.22, p=0.03) (Fig. 1B). Consequently, a higher viral load slightly was correlated with a lower CD4 count at the first visit (R=-0.22, p=0.033) (Fig. 1C).

Disease progression was analyzed in 82 patients. None of the patients had AIDS-defining events. Estimates of the risk of disease progression were 50.6% at 24 weeks, 61.0% at 48 weeks, 67.0% at 96 weeks, and 82.2% at 144 weeks

Table 1. **Baseline Characteristics of 108 Patients with Primary HIV-1 Infection in this Study**

Characteristics	Total number or mean (±SD) or %	Hospitalized patients (n = 58)	Non-hospitalized patients (n = 50)	p
Age (year)	31.8±8.48	32±9.07	31±7.82	NS
Sex				
Male	102	56	46	NS
Female	6	2	4	NS
Predisposing factor				
MSM	97	53	44	NS
Heterosexual	8	3	5	NS
IDU	1	0	1	NS
Unknown	2	2	0	NS
PMH of STD	75 (69.7)	44 (40.4)	31 (29.3)	NS
Syphilis	49 (45.5)	27 (25.3)	21 (20.2)	NS
Acute hepatitis A	11 (10.1)	6 (6.1)	5 (4.0)	NS
Acute hepatitis B	36 (33.3)	22 (20.2)	14 (13.1)	NS
Amebiasis	10 (9.1)	9 (8.0)	1 (1.1)	0.035
Others	7 (6.1)	2 (2.0)	5 (4.1)	NS
No. of symptoms	4.75±1.99	4.98±1.94	4.48±2.04	NS
Duration of symptoms (days)	23.2±14.8	27.8±13.1	18.0±15.1	0.001
Laboratory findings				
CD4 count/μL	390.0±220.1	356.1±204.1	443.7±236.0	0.06
HIV RNA $\log_{10}$/mL	4.81±0.78	5.03±0.68	4.48±0.81	0.001
STI trial*	26	12	14	NS

*Patients enrolled in a clinical trial of structured treatment interruptions in recently HIV-1-infected patients. Abbreviations; MSM: men who have sex with men, PMH of STD: past medical history of sexual transmitted diseases, STI: structured treatment interpretations, IDU: intravenous drug user, Others: genital herpes infection, chlamydial urethral infection condyloma acuminata, NS: not significant

Data are presented as mean ± SD or percentage (%) unless otherwise indicated

Table 2. **Symptoms and Physical Findings Observed in the Patients with >10% Frequencies (n=108)**

Symptoms and physical findings	frequency (%)
Fever	91
Lymphadenopathy	63
Pharyngitis	53
Rash	50
Diarrhea	37
Fatigue	32
Headache	26
Myalgia	20
Weight loss	19
Nausea	16
Appetite loss	14
Neurological sign	13
Hepatomegaly	13
Thrush	12

(Fig. 2). Eighteen of 34 (53.3%) patients with an initial CD 4 cell count below 350 cells/μL had immunologic progression at the first visit. Their CD4 counts never increased above 350/μL until initiation of HAART. Forty-eight (58.5%) required initiation of HAART in this study. The reasons for the initiation of HAART were severe clinical symptoms related to PHI in 16 patients and immunologic progression in 32 patients. The median CD4 count of those patients at initiation of HAART was 215/μL (range, 52-858).

We analyzed the clinical course in 66 patients (excluding 26 patients who enrolled in a clinical trial of structured treatment interruptions in PHI and 16 patients who received HAART for PHI) to determine the factors associated with disease progression. Half of these patients (33 patients) required hospitalization. As shown in Fig. 3A, the mean time to disease progression of the hospitalized patients [57.4 weeks, 95% confidence interval (95%CI); 34.9-79.8 weeks] was shorter than that of the non-hospitalized (33 patients, 94.4 weeks, 95%CI; 71-117 weeks, p=0.002). Among the 32 patients with CD4 count >350/μL at first visit, 24% had documented disease progression within 1 year, whereas among 34 patients with CD4 count <350/μL at first visit, 76.4% showed disease progression (Fig. 3B). The mean times to disease progression for the two groups were 111.9 weeks (95%CI; 92.8-131) and 39.5 weeks (95%CI; 18.6-60.5), respectively (p<0.001). Disease progression in 39 patients with high viral load (≥5.0 $\log_{10}$/mL) was not significantly different (p=0.41) from that in 27 patients with low viral load (<5.0 $\log_{10}$/mL) (Fig. 3C). The number of symptoms was not significantly different in each group (Fig. 3D). The mean time to disease progression was 69.8 weeks (95% CI; 47.2-92.5) in patients with a high viral load and 80.4 weeks (95%CI; 54.9-105.8) in those with a low viral load.

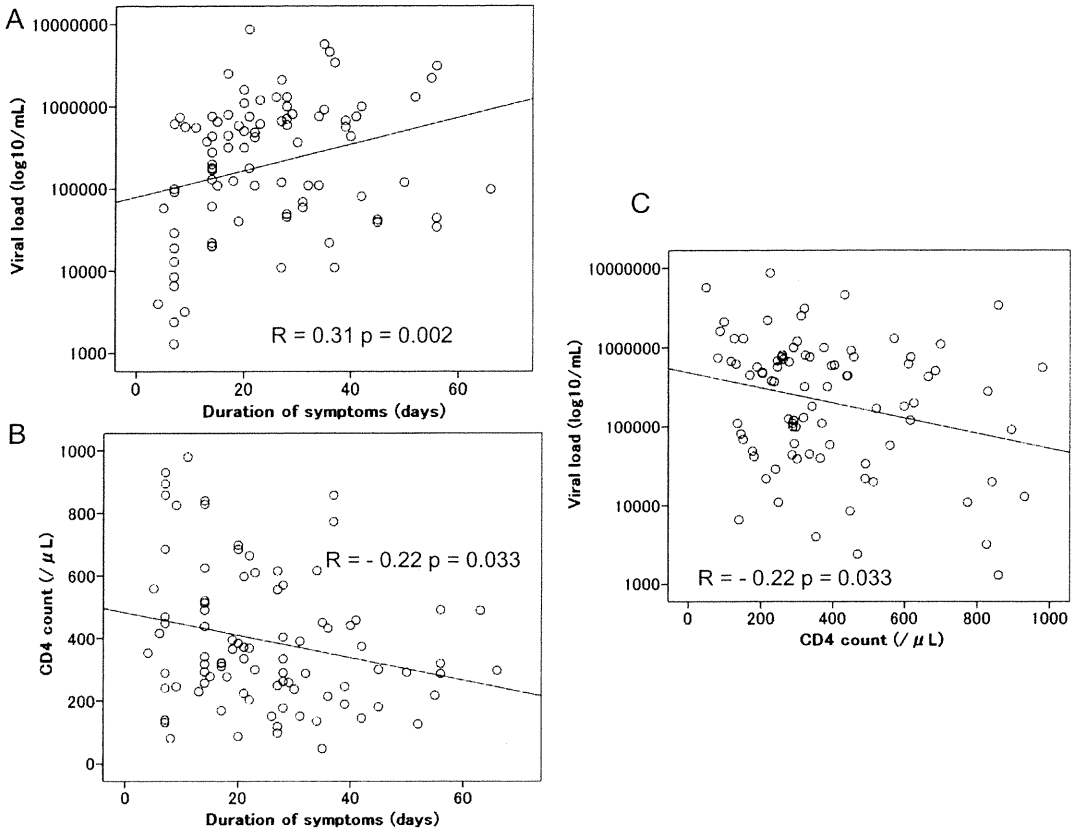

Figure 1. **Correlations among plasma viral load, CD4 count, and clinical symptoms. A; Plasma viral load correlated with duration of symptoms (R=0.31, p=0.002). B; CD4 count correlated inversely with duration of symptoms (R=-0.22, p=0.033). C; plasma viral load correlated inversely with CD4 count (R=-0.22, p=0.033).**

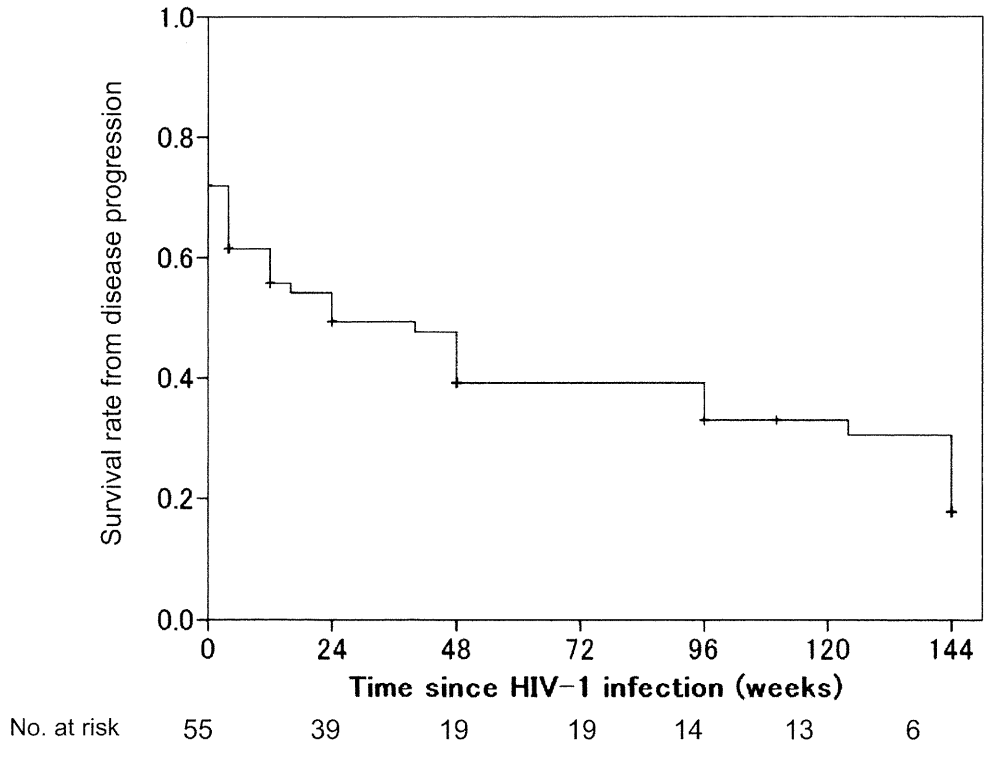

Figure 2. **Progression-free survival in 82 patients. Progression was defined as CD4 count <350/μL or initiation of HAART. No. at risk: the number of CD4 count >350/μL or HAART naïve patients**

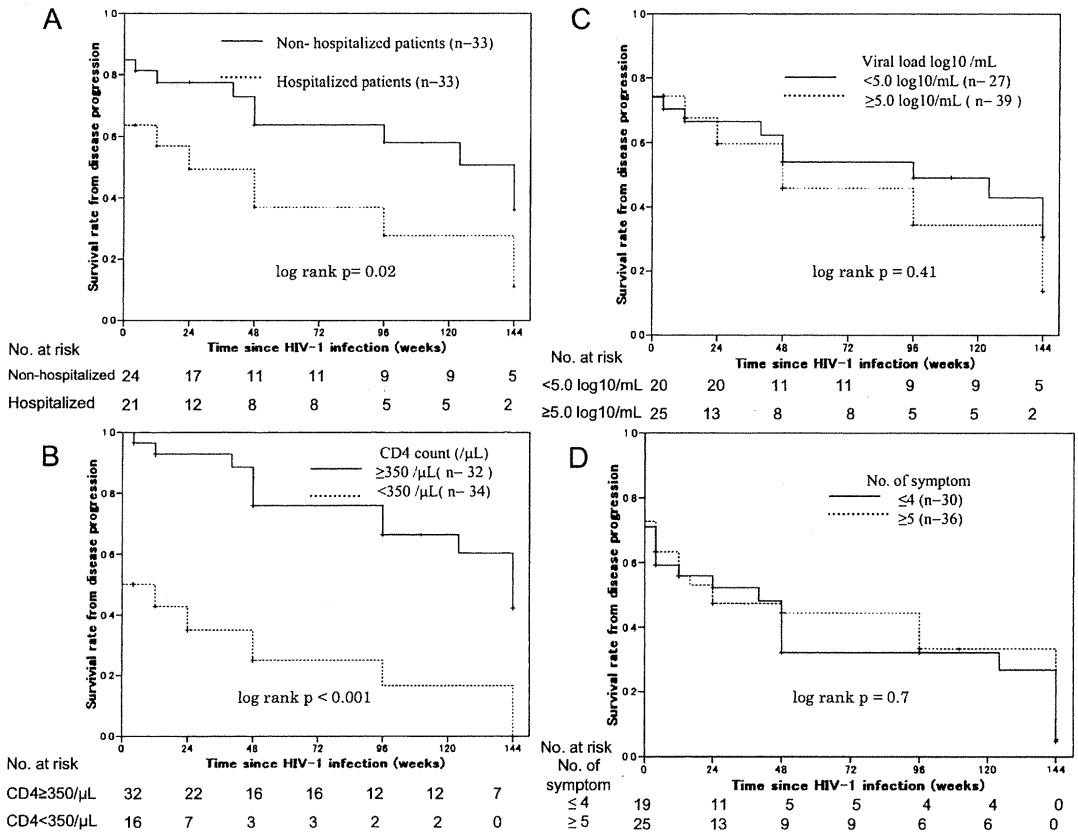

Figure 3. Progression-free survival among 66 patients according to rate of hospitalization, baseline CD4 count, and viral load. No. at risk: the number of CD4 count >350/μL or HAART naïve patients. A; Solid line: patients who required hospitalization due to PHI, dashed line: patients who did not require hospitalization (p=0.02, by log-rank test). B; Solid line: patients with CD4 count >350/μL at first visit, dashed line: patients with CD4 count <350/μL (p<0.001). C; Solid line: patients with viral load <5.0 log_{10}/mL, dashed line: patients with viral load ≥5.0 log_{10}/mL (p=0.41). Disease progression was defined as CD4 count <350/μL or initiation of HAART. D; Solid line: patients with the number of PHI symptoms ≤4, dashed line: patients with the number of PHI symptoms ≥5 (p=0.7, by log-rank test).

Comparison of percentage of recently infected patients with CD4 counts >350/μL at 3 years after infection and that of hemophiliacs as the first HIV-1 infected population in Japanese is shown in Fig. 4. The percentage (13.5%) of recently infected patients was significantly lower than that (47.6%) of Japanese hemophiliacs (p<0.001), clearly indicating the rapid decline of CD4 count in recently infected patients.

Discussion

In this study, we demonstrated rapid disease progression of symptomatic PHI Japanese patients in this decade. However, when we divided our study subjects into two groups according to the first half (1997-2002) and the latter half (2003-2007), disease progression of each group was not different (data not shown). In contrast, disease progression surrogated with natural CD4 decline of recently infected patients was significantly accelerated compared with Japanese hemophiliacs infected with HIV-1 before 1985. However, there are two quite different backgrounds; one is the route of infection and the other is the year of infection. Almost all hemophiliac patients are also co-infected with hepatitis C but do not have other sexually transmitted diseases (STDs). In contrast, most patients in the present study were infected via homosexual intercourse with many other STDs that may facilitate acceleration of the disease progression (7). In the present study, 69.7% patients had a past medical history of STDs, and the mean number of STDs was 1.08/patient (0: 31.3%, 1: 37.4%, 2: 23.2%, 3: 8.1%). In this regard, most published data on disease progression were obtained from men who have sex with men (MSM) cohorts (1, 2). Therefore, it is unlikely that the recent rapid disease progression is due to Japanese MSM. Whether or not the rapid disease progression in the recently HIV-1-infected Japanese can be generalized is to be elucidated in future studies.

Some HLA types are protective against disease progression such as HLA-B57 (19) and HLA-B51 (20) because HLA-restricted cytotoxic T lymphocytes (CTLs) play an important role on viral control. On the other hand, virus can easily escape from CTLs (17, 21). In some prevalent HLA types, escape virus can transmit and accumulate in the population (21). In this situation, some HLA types are no more

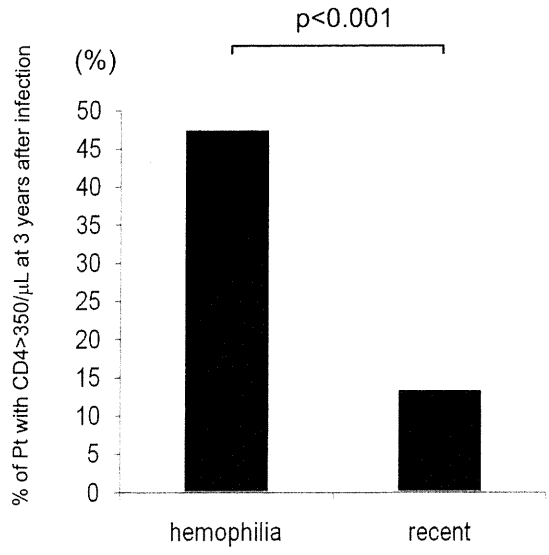

Figure 4. **Comparison of percentage of previously and recently infected patients with CD4 counts >350/μL at 3 years after infection. In this analysis, Japanese hemophiliacs (designated "hemophilia" in the figure) were regarded as a previously infected patient, because they were infected with HIV-1 before 1985. The number of hemophiliacs was 42 patients. The eligible number of recently infected patients (designated "recent" in the figure) was 59 patients; infected with HIV-1 after 1997, untreated, and CD4 count at 3 years after infection.**

protective. The HLA distribution is different in Americans compared to Japanese. Another possible hypothesis for the different disease progression is that Japanese hemophiliacs were exposed to HIV-1 through contaminated blood products imported from US as the first Japanese population infected with the virus around 1983. However, in recent years, most HIV-1 infection in Japanese is transmitted from Japanese patients. It can be postulated that current HIV-1 in Japan has adapted to the Japanese population, indicating acquisition and accumulation of escape virus from immune pressure of the otherwise protective HLA in Japanese population (21). From a negative point of view, the situation is similar to the epidemic of drug-resistance virus in treatment of naïve patients (22). The clinical relevance of the prevalence of immune escape virus in Japanese is a potentially serious matter in terms of the natural course of HIV-1 infection.

In the present study, all patients have had at least one symptom associated with PHI. During the follow-up period, no patient developed AIDS, whereas around 70% of the patients experienced immunologic progression as defined by a CD4 count <350/μL. It is noteworthy that the majority of these patients exhibited immunologic progression within 3 years and, surprisingly, >60% of them were documented within the first year. HAART was initiated in nearly 60% of patients during this period, including initiation for PHI-related severe symptoms in 20% of these patients. Previous studies on PHI have suggested that the number, duration, and/or severity of symptoms can predict faster disease progression to AIDS (23, 24). Our findings are compatible with these previous studies. Considered together, these results suggest that the duration of illness rather than the number of symptoms is more likely to be a major determinant of immunological progression. The estimated risks of disease progression were more than 50% by week 24 and 80% by week 144. Comparison with those observed elsewhere during the natural course of HIV-1 infection (24), these disease progression rates are surprisingly high. Among the patients with CD4 counts >350/μL at first visit, a quarter of them showed disease progression within 1 year. In contrast, in patients with CD4 count <350/μL, three quarters of them showed disease progression within the same period. Goujard et al (25) suggested possible recovery of CD4 count after the primary infection phase even in patients with very low count because it fluctuates during that period. In contrast, our results suggest that patients with a CD4 count of <350/μL during primary infection should be monitored carefully because spontaneous recovery of CD4 cell count during primary infection was rare. This cautionary remark could also apply to patients with a CD4 count of >350/μL because they exhibited nearly 60% risk of disease progression within 3 years. These observations may allow more targeted clinical monitoring and timely initiation of HAART. The impact of a short-term HAART during symptomatic primary infection on the subsequent disease progression needs to be elucidated in future study.

Although we included all recent seroconverters during the study period, it could be argued that this study carries some institution bias (i.e., a high proportion of cases with severe disease). However, the present finding of a surprisingly rapid disease progression in our patient population is new. Whether or not the natural course of disease progression has recently become accelerated in other countries or other cohorts is a matter of great interest.

The authors state that they have no Conflict of Interest (COI).

Acknowledgement

The authors thank all clinical staffs of the AIDS Clinical Center. This study was supported in part by a Grant-in-Aid for AIDS Research from the Ministry of Health, Labour, and Welfare of Japan.

References

1. Collaborative Group on AIDS Incubation and HIV Survival. Time from HIV-1 seroconversion to AIDS and death before widespread use of highly-active antiretroviral therapy: a collaborative reanalysis. Lancet **355**: 1131-1137, 2000.
2. Lyles RH, Munoz A, Yamashita TE, et al. Natural history of human immunodeficiency virus type 1 viremia after seroconversion and proximal to AIDS in a large cohort of homosexual men. Multicenter AIDS cohort study. J Infect Dis **181**: 872-880, 2000.
3. Crum-Cianflone N, Eberly L, Zhang Y, et al. Is HIV becoming more virulent? Initial CD4 counts among HIV seroconverters during the course of the HIV epidemic: 1985-2007. Clin Infect Dis **48**: 1285-1292, 2009.

4. Muller V, Maggiolo F, Suter F, et al. Increasing clinical virulence in two decades of the Italian HIV epidemic. PLoS Pathog **5**: e1000454, 2009.
5. Carrington M, O'Brien SJ. The influence of HLA genotype on AIDS. Annu Rev Med **54**: 535-551, 2003.
6. McShane H. Co-infection with HIV and TB: double trouble. Int J STD AIDS **16**: 95-100, 2005.
7. Palacios R, Jimenez-Onate F, Aguilar M, et al. Impact syphilis infection on HIV viral load and CD4 cell counts in HIV-infected patients. J Acquir Immun Defic Syndr **44**: 356-359, 2007.
8. Duncombe C, Kerr SJ, Ruxrungtham K, et al. HIV disease progression in a patient cohort treated via a clinical research network in a resource limited setting. AIDS **28**: 169-178, 2005.
9. Pedersen C, Katzenstein T, Nielsen C, et al. Prognostic value of serum HIV-RNA levels at virologic steady state after seroconversion: relation to CD4 cell count and clinical course of primary infection. J Acquir Immune Defic Syndr Hum Retrovirol **16**: 93-99, 1997.
10. Vanhems P, Hirschel B, Phillips AN, et al. Incubation time of acute human immunodeficiency virus (HIV) infection and duration of acute HIV infection are independent prognostic factors of progression to AIDS. J Infect Dis **182**: 334-337, 2000.
11. Vanhems P, Lanbert J, Cooper DA, et al. Severity and prognosis of acute human immunodeficiency virus type 1 illness: a dose-response relationship. Clin Infect Dis **26**: 323-329, 1998.
12. Sterling T, Vlahov D, Astemborski J, et al. Initial plasma HIV-1 RNA levels and progression to AIDS in women and men. N Engl J Med **344**: 720-725, 2001.
13. Henrard DR, Daar E, Farzadegan H, et al. Virologic and immunologic characterization of symptomatic and asymptomatic primary HIV-1 infection. J Acquir Immune Defic Syndr Hum Retrovirol **9**: 305-310, 1995.
14. Schacker TW, Hughes JP, Shea T, et al. Biological and virologic characteristics of primary HIV infection. Ann Intern Med **128**: 613-620, 1998.
15. Lefrere JJ, Roudot-Thoraval F, Mariotti M, et al. The risk of disease progression is determined during the first year of human immunodeficiency virus type 1 infection. J Infect Dis **177**: 1541-1548, 1998.
16. Fujiwara M, Tanuma J, Koizumi H, et al. Different abilities of escape mutant-specific cytotoxic T cells to suppress replication of escape mutant and wild-type human immunodeficiency virus type 1 in new hosts. J Virol **82**: 138-147, 2008.
17. Tanuma J, Fujiwara M, Teruya K, et al. HLA-A*2402-restricted HIV-1 specific T lymphocytes and escape mutation after ART with structured treatment interruptions. Microbes Infect **10**: 689-698, 2008.
18. Thompson MA, Aberg JA, Cahn P, et al. Antiretroviral treatment of adult HIV infection; 2010 recommendations of the international AIDS Society-USA Panel. JAMA **304**: 321-333, 2010.
19. Goulder PJ, Bunce M, Krausa P, et al. Novel, cross-restricted, conserved, and immunodominant cytotoxic T lymphocyte epitopes in slow progressors in HIV type 1 infection. AIDS Res Hum Retroviruses **10**: 1691-1698, 1996.
20. Kawashima Y, Kuse N, Gatanaga H, et al. Long-term control of HIV-1 in hemophiliacs carrying slow-progressing allele HLA-B* 5101. J Virol **84**: 7151-7160, 2010.
21. Kawashima Y, Pfafferott K, Frater J, et al. Adaptation of HIV-1 to human leukocyte antigen class I. Nature **458**: 641-645, 2009.
22. Little SJ, Holte S, Routy JP, et al. Antiretroviral-drug resistance among patients recently infected with HIV. N Engl J Med **347**: 385-394, 2002.
23. Vanhems P, Lambert J, Cooper DA, et al. Severity and prognosis of acute immunodeficiency virus type 1 illness: a dose-response relationship. Clin Infect Dis **26**: 323-329, 1998.
24. Lavreys L, Baeten JM, Chohan V, et al. Higher set point plasma viral load and more-severe acute HIV type 1 (HIV-1) illness predict mortality among high-risk HIV-1-infected African women. Clin Infect Dis **42**: 1333-1339, 2006.
25. Goujard C, Bonarek M, Meyer L, et al. CD4 cell count and HIV DNA level are independent predictors of disease progression after primary HIV type 1 infection in untreated patients. Clin Infect Dis **42**: 709-715, 2006.

Bioorganic & Medicinal Chemistry Letters 22 (2012) 2308–2311

Contents lists available at SciVerse ScienceDirect

Bioorganic & Medicinal Chemistry Letters

journal homepage: www.elsevier.com/locate/bmcl

Substituent effects on P2-cyclopentyltetrahydrofuranyl urethanes: Design, synthesis, and X-ray studies of potent HIV-1 protease inhibitors

Arun K. Ghosh [a,*], Bruno D. Chapsal [a], Melinda Steffey [a], Johnson Agniswamy [b], Yuan-Fang Wang [b], Masayuki Amano [c], Irene T. Weber [b], Hiroaki Mitsuya [c,d]

[a] Department of Chemistry and Department of Medicinal Chemistry, Purdue University, West Lafayette, IN 47907, USA
[b] Department of Biology, Molecular Basis of Disease, Georgia State University, Atlanta, GA 30303, USA
[c] Departments of Hematology and Infectious Diseases, Kumamoto University Graduate School of Medical and Pharmaceutical Sciences, Kumamoto 860-8556, Japan
[d] Experimental Retrovirology Section, HIV and AIDS Malignancy Branch, National Cancer Institute, National Institutes of Health, Bethesda, MD 20892, USA

ARTICLE INFO

Article history:
Received 28 December 2011
Accepted 17 January 2012
Available online 2 February 2012

Keywords:
HIV-1 protease inhibitors
P2 ligand
Drug resistance
Design and synthesis
X-ray crystal structure

ABSTRACT

The design, synthesis, and biological evaluation of novel C3-substituted cyclopentyltetrahydrofuranyl (Cp-THF)-derived HIV-1 protease inhibitors are described. Various C3-functional groups on the Cp-THF ligand were investigated in order to maximize the ligand-binding site interactions in the flap region of the protease. Inhibitors **3c** and **3d** have displayed the most potent enzyme inhibitory and antiviral activity. Both inhibitors have maintained impressive activity against a panel of multidrug resistant HIV-1 variants. A high-resolution X-ray crystal structure of **3c**-bound HIV-1 protease revealed a number of important molecular insights into the ligand-binding site interactions.

HIV-1 protease inhibitors continue to be a critical component of frontline therapy in the treatment of HIV patients.[1–3] Our continuing studies on the structure-based design of inhibitors targeting the protein backbone led to the discovery of a variety of novel HIV-1 protease inhibitors (PIs) with broad-spectrum activity against multidrug-resistant HIV-1 variants.[4–8] We recently reported various C3-functionalized cyclopentyltetrahydrofuran (Cp-THF)-derived P2-ligands designed to specifically interact with the flap Gly48 amide NH in the S2-subsite of the HIV-1 protease.[9] One of these inhibitors, **2** (Fig. 1), containing a 3-(*R*)-hydroxy group on the Cp-THF core displayed exceptionally potent enzyme inhibitory (K_i = 5 pM) and antiviral activity (IC_{50} = 2.9 nM). This inhibitor also exhibited potent activity against a panel of multidrug-resistant HIV-1 variants. The X-ray crystal structure of **2**-bound HIV protease revealed an extensive hydrogen-bonding network with the enzyme backbone.[9] Of particular interest, the 3-(*R*)-hydroxy group of the Cp-THF ligand was involved in an interesting water-mediated interaction with the backbone NH amide bond of Gly48. This specific interaction was not present in inhibitor **1**. These additional interactions observed with **2** may have contributed toward its impressive drug resistance profile. [9]

Based upon the **2**-bound X-ray crystal structure of HIV-1 protease, and given the significant gain in antiviral activity observed with the addition of C3-polar substituents on the Cp-THF P2 ligand, we subsequently speculated that N-substituted functionalities, particularly *N*-acyl, *N*-carbamate or *N*-sulfonyl derivatives could function as both a hydrogen-bonding donor and acceptor. The NH proton could conceivably form an effective hydrogen bond with the proximal Gly48 carbonyl while amide or urethane carbonyl oxygen may form an additional interaction with the protease backbone. Indeed, our previous exploration of such hydrogen bond donor and acceptor functionalities on P2-ligand frameworks led to remarkably potent HIV-1 protease inhibitors with broad-spectrum antiviral activity. [4–9] Herein, we report the design, synthesis and biological evaluation of a series of HIV-1 protease inhibitors with C-3 substituted Cp-THF as the P2-ligand. A number of inhibitors exhibited exceptionally potent antiviral activity against a panel of multidrug-resistant HIV-1 variants. A protein-ligand X-ray crystal structure also provided important molecular insight into the ligand-binding site interactions.

The synthesis of ligands containing various N-substituents with either stereochemistry at C3 was accomplished starting from our previously reported optically active ketone intermediate **4**[10] as shown in Scheme 1. Ketone **4** was converted to methyloxime derivatives **5** in 96% yield. Reduction of **5** with a mixture of Pd/C and Raney-Ni under hydrogen pressure (80 psi) provided the corresponding amine as a 3:1 diastereomeric mixture.[11] The amine mixture was reacted with Ac_2O in the presence of Et_3N and a catalytic amount of DMAP to yield a mixture of isomeric TBS-protected

* Corresponding author. Tel.: +1 765 494 5323; fax: +1 765 496 1612.
E-mail address: akghosh@purdue.edu (A.K. Ghosh).

0960-894X/$ - see front matter © 2012 Elsevier Ltd. All rights reserved.
doi:10.1016/j.bmcl.2012.01.061

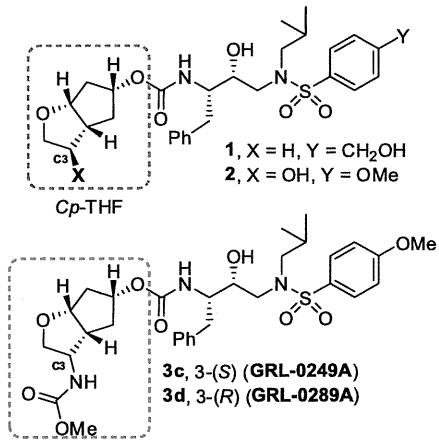

Figure 1. Structure of protease inhibitors **1,2, 3c–d.**

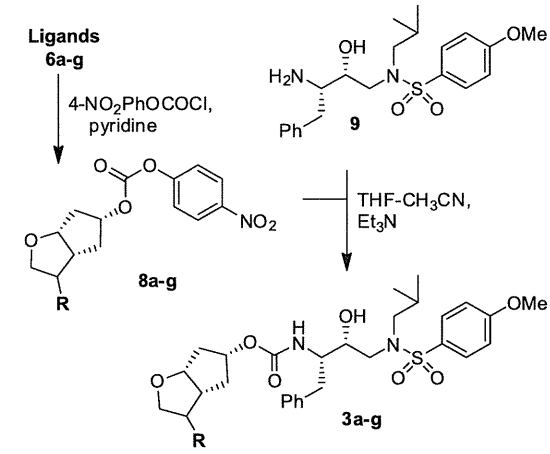

Scheme 2. Synthesis of protease inhibitors **3a–g.**

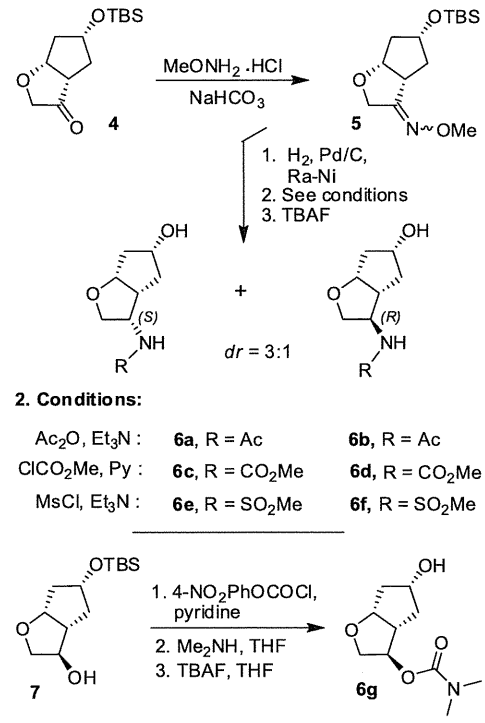

Scheme 1. Synthesis of C3-substituted ligands **6a–g.**

amide intermediates in 80% yield. Treatment of the respective amides with TBAF in THF and chromatographic separation furnished diastereomerically pure ligands **6a** and **6b** in excellent yield. Similarly, the amine mixture was treated with methyl chloroformate and pyridine, or mesyl chloride and Et_3N to afford the corresponding carbamates and sulfonamides. Treatment of the respective crude mixtures with TBAF in THF followed by chromatographic separation afforded diastereoisomeric *N*-carbamate ligands **6c** and **6d**, and *N*-mesyl ligands **6e** and **6f**, respectively. The assignment of stereochemistry on the ligands was carried out by NOE or NOESY experiments of the corresponding mixed activated carbonates **8a**, **8c**, and **8e**. To probe the importance of the free NH, we have synthesized ligand **6g** containing a 3-(*R*)-*O*-dimethylaminocarbamate group. This was synthesized in three consecutive steps starting from our previously reported optically active alcohol **7**.[9] Treatment of **7** with 4-nitrophenyl chloroformate in the presence of pyridine furnished the corresponding mixed activated carbonate. The resulting carbonate was reacted with a bubbling stream of Me_2NH gas to provide the corresponding TBS-protected ligand. Removal of the TBS-group with TBAF furnished ligand **6g** in excellent yield.

For the synthesis of HIV protease inhibitors, all ligand alcohols **6a–g** were reacted with 4-nitrophenyl chloroformate in the presence of pyridine in CH_2Cl_2 to furnish the corresponding mixed activated carbonates **8a–g** (Scheme 2).[9,10] The activated carbonates were then reacted with previously reported hydroxyethylamine isostere **9**[9] in the presence of Et_3N in THF/CH_3CN for 2–4 days to give corresponding inhibitors **3a–g**.

Inhibitors **3a–g** were initially tested in enzyme inhibitory assays using the method developed by Toth and Marshall,[12] and then evaluated for in vitro antiviral assays. Results are shown in Table 1. All inhibitors displayed impressive inhibitory potency and high antiviral activity. Inhibitors **3a** and **3b** that, contain a 3-(*S*)- or 3-(*R*)-*N*-acetyl substituent on the Cp-THF ligand, exhibited similar potency (7.4 and 7.5 pM, respectively). Interestingly, the stereochemistry at C3 seemed to have little effect. Inhibitor **3c** with a 3-(*S*)-*N*-methoxycarbonyl displayed the most impressive enzyme and antiviral potency (K_i = 1.8 pM and IC_{50} = 1.6 nM). The isomeric inhibitor **3d** provided slightly lower potency. Inhibitors **3e** and **3f** that contain a 3-*N*-mesyl on the Cp-THF ligand, showed a substantial reduction in activity probably due to the increase in steric bulk created by the *N*-mesyl group. Inhibitor **3g** that contains an O-substituted dimethylaminocarbamate in place of N-substituted carbamate at C3 provided a good antiviral activity, similar to that of **3d**.

Inhibitors **3c** and **3d**, were further evaluated against a panel of multidrug-resistant (MDR) HIV-1 variants and their antiviral activities were compared to clinically available PI, darunavir (DRV).[6,13] Results are shown in Table 2. All inhibitors exhibited low nanomolar EC_{50} values against the wild-type HIV-$1_{ERS104pre}$ laboratory strain, isolated from a drug-naïve patient.[13] Inhibitor **3d** had the most potent activity (EC_{50} = 3 nM) similar to that of DRV. When tested against a panel of multidrug-resistant HIV-1 strains, the EC_{50} of **3d** remained in the low nanomolar value range (15–24 nM) and its fold-changes in activity were similar to those observed with DRV.[6,13] Interestingly, inhibitor **3c**, with the opposite (*S*) stereochemistry at C3, displayed slightly lower antiviral activities against all viral strains compared to **3d**. However, the fold-changes in EC_{50} for **3c** remained low (<3) against all MDR HIV-1 viruses. The fold-changes contrasted with those of **3d** and even DRV, for which the respective EC_{50}'s increased by a factor of at least three against the MDR viruses examined.[14]

In order to gain molecular insights on the ligand-binding site interactions responsible for the potent activity and excellent resistance profile of **3c**, we have determined the X-ray crystal structure

Table 1
Structures and potency of inhibitors **3a–g**[a]

Entry	Inhibitor structure	K_i (pM)	IC_{50} (nM)[b]
1	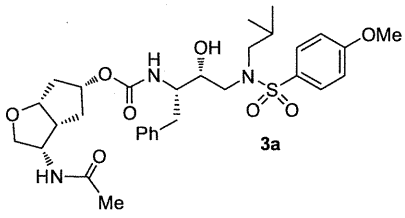 **3a**	7.4	25
2	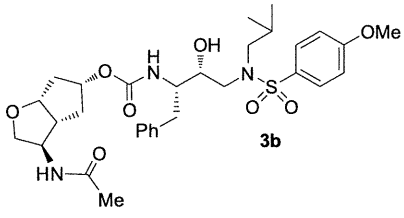 **3b**	7.5	31
3	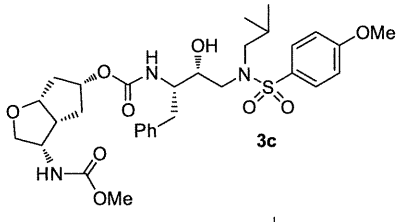 **3c**	1.8	1.6
4	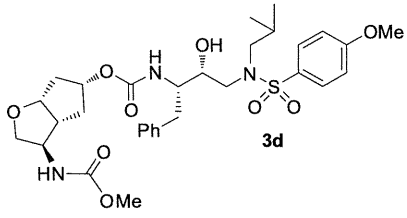 **3d**	4.0	4.6
5	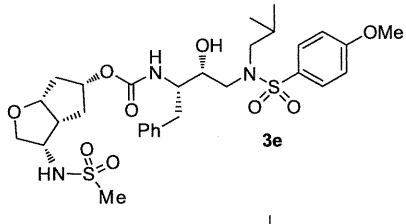 **3e**	32	28
6	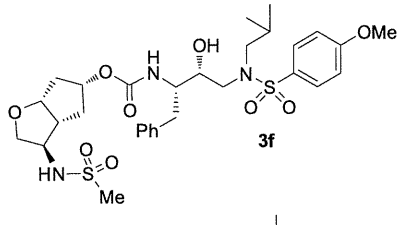 **3f**	180	50
7	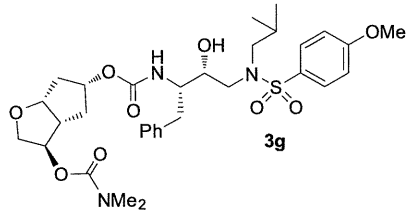 **3g**	20	4.7

[a] Values are the mean value of at least two experiments.
[b] Human T-lymphoid (MT-2) cells (2×10^3) were exposed to 100 $TCID_{50}$ of HIV-1_{LAI} and cultured in the presence of each PI, and IC_{50} values were determined using the MTT assay. The IC_{50} values of amprenavir (APV), saquinavir (SQV), indinavir (IDV), and darunavir (DRV) were 0.03, 0.015, 0.03, and 0.003 μM, respectively.

of the HIV wild-type protease complexed with **3c** (Fig. 2).[15] The structure was refined to an R-factor of 14.9% and a resolution of

Table 2
Comparison of the antiviral activity of **3c**, **3d**, and DRV against multidrug-resistant HIV-1 variants

Virus[a]	EC_{50} (μM) ±SDs, (fold-change)[b]		
	3c	**3d**	**DRV**
HIV-$1_{ERS104pre}$ (wt)	0.029 ± 0.002	0.003 ± 0.001	0.004 ± 0.001
HIV-$1_{MDR/B}$ (X4)	0.075 ± 0.011 (3)	0.018 ± 0.003 (6)	0.019 ± 0.006 (5)
HIV-$1_{MDR/C}$ (X4)	0.030 ± 0.006 (1)	0.015 ± 0.005 (5)	0.011 ± 0.003 (3)
HIV-$1_{MDR/G}$ (X4)	0.039 ± 0.001 (1)	0.020 ± 0.005 (7)	0.011 ± 0.002 (3)
HIV-$1_{MDR/TM}$ (X4)	0.074 ± 0.006 (3)	0.024 ± 0.004 (8)	0.028 ± 0.001 (7)

[a] Amino acid substitutions identified in the protease-encoding region of HIV-$1_{ERS104pre}$, HIV-$1_{MDR/B}$, HIV-$1_{MDR/C}$, HIV-$1_{MDR/G}$, HIV-$1_{MDR/TM}$ compared to the consensus type B sequence cited from the Los Alamos database include L63P in HIV-$1_{ERS104pre}$; L10I, K14R, L33I, M36I, M46I, F53I, K55R, I62V, L63P, A71V, G73S, V82A, L90M, I93L in HIV-$1_{MDR/B}$; L10I, I15V, K20R, L24I, M36I, M46L, I54V, I62V, L63P, K70Q, V82A, and L89M in HIV-$1_{MDR/C}$; L10I, V11I, T12E, I15V, L19I, R41K, M46L, L63P, A71T, V82A, and L90M in HIV-$1_{MDR/G}$; L10I, K14R, R41K, M46L, I54V, L63P, A71V, V82A, L90M, I93L in HIV-$1_{MDR/TM}$. HIV-$1_{ERS104pre}$ served as a source of wild-type HIV-1.
[b] EC_{50} values were determined by using PHA-PBMs as target cells and the inhibition of p24 Gag protein production for each drug was used as an endpoint. The numbers in parentheses represent the fold-change in EC_{50} values for each isolate compared to the EC_{50} values for the wild-type HIV-$1_{ERS104pre}$. All assays were conducted in duplicate, and the data shown represent mean values (±1 standard deviations) derived from the results of two or three independent experiments. PHA-PBMs were derived from a single donor in each independent experiment. DRV (darunavir).

1.23 Å. The inhibitor is bound to the protease dimer in two orientations related by a 180° rotation, with a 50/50 relative occupancy. The protease backbone structure showed a very low rms deviation of 0.11 Å for all Cα carbons compared to the protease complexes of **2**[9] or DRV.[21] As shown in Figure 2, the inhibitor interactions in the protease binding site extend from S2 to S2′ protease subsites and consist of a series of strong hydrogen bonds and weaker C–H···O and C–H···π interactions similar to those previously described for DRV,[21] or inhibitor **2**.[9] The Cp-THF cyclic oxygen forms a strong hydrogen bond with the backbone amide NH of Asp29 in the protease S2-binding site, similar to that previously observed with other Cp-THF-based inhibitors **1**[5] and **2**.[9] Critical differences, however, are observed with the additional interactions that the 3-(*S*)-*N*-methoxycarbonyl amino substituent on the Cp-THF makes throughout the S2–S3 subsites. As shown in Figure 2, the carbamate NH forms a strong hydrogen bond with the Gly48 backbone carbonyl. The carbamate carbonyl is observed to interact with the Arg8′ guanidine side chain through a conserved water molecule. The methyl of the methoxy group then fits within the S3-hydrophobic pocket. The C3-*N*-methoxycarbonyl amino group creates a network of tight hydrogen bonds that literally links the protease flap region to the S2–S3 subsites' dimer interface. These new interactions and enthalpic nature of the additional hydrogen bonding created by the P2-ligand may certainly exert an enhanced anchoring effect of the inhibitor into the S2-subsite and further stabilize the closed conformation of the protease–ligand complex.

In conclusion, we have reported the structure-based design of a series of highly potent HIV-1 protease inhibitors incorporating C3-substituted cyclopentyltetrahydrofuranyl urethanes as P2-ligands. Various C3-*N*-substituents were investigated in order to create multiple interactions in the S2-subsite of the protease and specifically with the protease flap region. Inhibitors **3c** and **3d** displayed remarkable inhibitory potency and antiviral activity. When tested against a panel of MDR HIV-1 strains, inhibitor **3d**, with a 3-(*R*)-methoxycarbonyl on the Cp-THF ligand, provided the most impressive EC_{50}s and fold-changes in activity which are comparable to those observed with clinically available DRV. Isomeric inhibitor **3c** displayed lower antiviral activity. However, it exhibited strikingly low fold-changes of antiviral activity when tested against MDR HIV-1 viruses. An X-ray crystal structure of the protease–**3c**

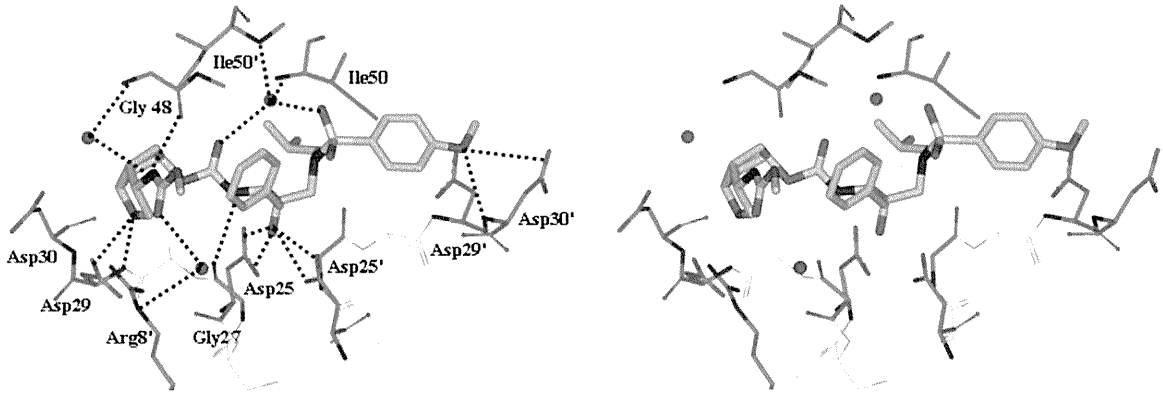

Figure 2. Stereoview of the X-ray structure of inhibitor **3c** (green)-bound HIV-1 protease (PDB code: 4DFG). All strong hydrogen bonding interactions are shown as dotted lines.

complex was determined at a 1.23 Å resolution. Inhibitor **3c** made extensive interactions throughout the protease binding site. The complex network of hydrogen-bonding interactions created by the *N*-methyl carbamate substituent in addition to those created by the isostere in the protease active site may account for the impressive antiviral activity and superb resistance profile observed with inhibitor **3c**. Further designs along this line and ligand optimization are currently underway.

Acknowledgements

This research was supported by the National Institutes of Health (Grant GM53386 to A.K.G. and Grant GM62920 to I.T.W.). This work was also supported by the Intramural Research Program of the Center for Cancer Research, National Cancer Institute, National Institutes of Health, and in part by a Grant-in-Aid for Scientific Research (Priority Areas) from the Ministry of Education, Culture, Sports, Science, and Technology of Japan (Monbu Kagakusho), a Grant for Promotion of AIDS Research from the Ministry of Health, Welfare, and Labor of Japan, and the Grant to the Cooperative Research Project on Clinical and Epidemiological Studies of Emerging and Reemerging Infectious Diseases (Renkei Jigyo) of Monbu-Kagakusho.

References and notes

1. Conway, B. *Future Virol.* **2009**, *4*, 39.
2. Hue, S.; Gifford, R. J.; Dunn, D.; Fernhill, E.; Pillay, D. *J. Virol.* **2009**, *83*, 2645.
3. Little, S. J.; Holte, S.; Routy, J. P.; Daar, E. S.; Markowitz, M.; Collier, A. C.; Koup, R. A.; Mellors, J. W.; Connick, E.; Conway, B.; Kilby, M.; Wang, L.; Whitcomb, J. M.; Hellmann, N. S.; Richman, D. D. N. *Engl. J. Med.* **2002**, *347*, 385.
4. Ghosh, A. K. *J. Med. Chem.* **2009**, *52*, 2163.
5. Ghosh, A. K.; Sridhar, P. R.; Leshchenko, S.; Hussain, A. K.; Li, J.; Kovalevsky, A. Y.; Walters, D. E.; Wedekind, J. E.; Grum-Tokars, V.; Das, D.; Koh, Y.; Maeda, K.; Gatanaga, H.; Weber, I. T.; Mitsuya, H. *J. Med. Chem.* **2006**, *49*, 5252.
6. Ghosh, A. K.; Dawson, Z. L.; Mitsuya, H. *Bioorg. Med. Chem. Lett.* **2007**, *15*, 7576.
7. Ghosh, A. K.; Leshchenko-Yashchuk, S.; Anderson, D. D.; Baldridge, A.; Noetzel, M.; Miller, H. B.; Tie, Y. F.; Wang, Y. F.; Koh, Y.; Weber, I. T.; Mitsuya, H. *J. Med. Chem.* **2009**, *52*, 3902.
8. Ghosh, A. K.; Chapsal, B. D.; Weber, I. T.; Mitsuya, H. *Acc. Chem. Res.* **2008**, *41*, 78.
9. Ghosh, A. K.; Chapsal, B. D.; Parham, G. L.; Steffey, M.; Agniswamy, J.; Wang, Y.-F.; Amano, M.; Weber, I. T.; Mitsuya, H. *J. Med. Chem.* **2011**, *54*, 5890.
10. Ghosh, A. K.; Chapsal, B. D.; Baldridge, A.; Ide, K.; Koh, Y.; Mitsuya, H. *Org. Lett.* **2008**, *10*, 5135.
11. Li, J. J.; Sutton, J. C.; Nirschl, A.; Zou, Y.; Wang, H.; Sun, C.; Pi, Z.; Johnson, R.; Krystek, S. R.; Seethala, R.; Golla, R.; Sleph, P. G.; Beehler, B. C.; Grover, G. J.; Fura, A.; Vyas, V. P.; Li, C. Y.; Gougoutas, J. Z.; Galella, M. A.; Zahler, R.; Ostrowski, J.; Hamann, L. G. *J. Med. Chem.* **2007**, *50*, 3015.
12. Toth, M. V.; Marshall, G. R. *Int. J. Pept. Protein Res.* **1990**, *36*, 544.
13. Koh, Y.; Nakata, H.; Maeda, K.; Ogata, H.; Bilcer, G.; Devasamudram, T.; Kincaid, J. F.; Boross, P.; Wang, Y.-F.; Tie, Y.; Volarath, P.; Gaddis, L.; Harrison, R. W.; Weber, I. T.; Ghosh, A. K.; Mitsuya, H. *Antimicrob. Agents Chemother.* **2003**, *47*, 3123.
14. Ghosh, A. K.; Chapsal, B. Mitsuya, H. In *Aspartic Acid Proteases as Therapeutic Targets*; Ghosh, A., Ed.; Wiley-VCH Verlag GmbH & Co. KGaA: Weinheim, 2010; pp 245–262.
15. The protein-ligand X-ray structure of **3c**-bound HIV-1 protease will be deposited in PDB (PDB ID: 4DFG). The HIV-1 protease was expressed and purified as previously described.[16] The protease–inhibitor complex was crystallized at room temperature by the hanging drop vapor diffusion method with well solutions of 1.2 M ammonium chloride and 0.1 M sodium acetate buffer (pH 4.8). Diffraction data were collected on a single crystal cooled to 90 K at SER-CAT BM beamline 22, Advanced Photon Source, Argonne National Laboratory (Chicago, IL, U.S.), with an X-ray wavelength of 1.0 Å and processed by HKL-2000 with R_{merge} of 7.2%. The PR structure was used in molecular replacement by PHASER[17] in the CCP4i suite[18] and refined to 1.45 Å resolution using SHELX-97 and COOT[19] for manual modification. PRODRG-2[20] was used to construct the inhibitor and the restraints for refinement. Alternative conformations were modeled, anisotropic atomic displacement parameters (*B* factors) were applied for all atoms including solvent molecules, and hydrogen atoms were added in the final round of refinement. The final refined solvent structure comprised two Cl^- ions and 142 water molecules.
16. Mahalingam, B.; Louis, J. M.; Hung, J.; Harrison, R. W.; Weber, I. T. *Proteins* **2001**, *43*, 455.
17. Shen, C.-H.; Wang, Y.-F.; Kovalevsky, A. Y.; Harrison, R. W.; Weber, I. T. *FEBS J.* **2010**, *277*, 3699.
18. Potterton, E.; Briggs, P.; Turkenburg, M.; Dodson, E. A. *Acta Crystallogr. Sect. D: Bio. Crystallogr.* **2003**, *59*, 1131.
19. Emsley, P.; Cowtan, K. *Sect. D: Bio. Crystallogr.* **2004**, *60*, 2126.
20. Schuttelkopf, A. W.; van Aalten, D. M. F. *Acta Crystallogr. Sect. D: Bio. Crystallogr.* **2004**, *60*, 1355.
21. Kovalevsky, A. Y.; Liu, F.; Leshchenko, S.; Ghosh, A. K.; Louis, J. M.; Harrison, R. W.; Weber, I. T. *J. Mol. Biol.* **2006**, *363*, 161.

Journal of Medicinal Chemistry

ARTICLE

pubs.acs.org/jmc

Design of HIV-1 Protease Inhibitors with C3-Substituted Hexahydrocyclopentafuranyl Urethanes as P2-Ligands: Synthesis, Biological Evaluation, and Protein−Ligand X-ray Crystal Structure†

Arun K. Ghosh,*[,‡] Bruno D. Chapsal,[‡] Garth L. Parham,[‡] Melinda Steffey,[‡] Johnson Agniswamy,[§] Yuan-Fang Wang,[§] Masayuki Amano,[∥] Irene T. Weber,[§] and Hiroaki Mitsuya[∥,⊥]

[‡]Departments of Chemistry and Medicinal Chemistry, Purdue University, West Lafayette, Indiana 47907, United States

[§]Department of Biology, Molecular Basis of Disease, Georgia State University, Atlanta, Georgia 30303, United States

[∥]Departments of Hematology and Infectious Diseases, Kumamoto University Graduate School of Medical and Pharmaceutical Sciences, Kumamoto 860-8556, Japan

[⊥]Experimental Retrovirology Section, HIV and AIDS Malignancy Branch, National Cancer Institute, National Institutes of Health, Bethesda, Maryland 20892, United States

Supporting Information

ABSTRACT: We report the design, synthesis, biological evaluation, and the X-ray crystal structure of a novel inhibitor bound to the HIV-1 protease. Various C3-functionalized cyclopentanyltetrahydrofurans (Cp-THF) were designed to interact with the flap Gly48 carbonyl or amide NH in the S2-subsite of the HIV-1 protease. We investigated the potential of those functionalized ligands in combination with hydroxyethylsulfonamide isosteres. Inhibitor **26** containing a 3-(*R*)-hydroxyl group on the Cp-THF core displayed the most potent enzyme inhibitory and antiviral activity. Our studies revealed a preference for the 3-(*R*)-configuration over the corresponding 3-(*S*)-derivative. Inhibitor **26** exhibited potent activity against a panel of multidrug-resistant HIV-1 variants. A high resolution X-ray structure of **26**-bound HIV-1 protease revealed important molecular insight into the ligand-binding site interactions.

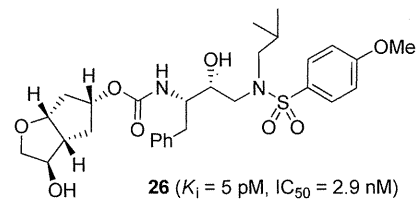

26 (K_i = 5 pM, IC_{50} = 2.9 nM)

INTRODUCTION

Human immunodeficiency virus 1 (HIV-1) protease inhibitors are critical components of antiretroviral therapies.[1,2] However, the emergence of drug resistance has raised serious questions about long-term treatment options.[3,4] Our structure-based design of inhibitors targeting the protein backbone has led to the discovery of a variety of novel HIV-1 protease inhibitors (PIs) with broad-spectrum activity against multidrug-resistant HIV-1 variants.[5,6] One of these inhibitors, darunavir (**1**, Figure 1), was approved by the FDA for the treatment of HIV/AIDS patients.[7−9] In an effort to address drug resistance, our inhibitor design strategy focused on maximizing active site interactions with the protease, particularly by promoting extensive hydrogen bonding interactions with backbone atoms throughout the active site.[5,6]

We have recently reported a number of potent inhibitors incorporating a stereochemically defined (3a*S*,5*R*,6a*R*)-hexahydro-2*H*-cyclopenta[*b*]furan-5-yl (Cp-THF) as the P2-ligand with a modified hydroxyethylsulfonamide isostere as in inhibitor **3**.[10] The X-ray crystal structure of **3**-bound HIV-1 protease revealed the formation of an extensive hydrogen-bonding network between the inhibitor and the active site. On the basis of this molecular insight, we subsequently incorporated a stereochemically defined lactam at the P1′-position to further enhance backbone interactions.[11] Interestingly, the resulting inhibitor **4** retained full potency against a range of multidrug-resistant HIV-1 variants.[12] The X-ray structural studies of **4**-bound HIV-1 protease evidenced enhanced backbone interactions with the Gly27′ carbonyl at the S1′-subsite. The Cp-THF ligand appears to fit within the S2-subsite, and the cyclic ether oxygen is involved in a close hydrogen bonding interaction with the backbone NH of Asp29 (2.8 Å). On the basis of this molecular insight, we have now investigated structural modifications of the Cp-THF ligand to further optimize ligand binding, particularly hydrogen bonding ability, in the S2-subsite. The X-ray structure of **3**-bound HIV-1 protease indicated that the C3 methylene of the Cp-THF is in proximity to the protease flap region. In fact, the X-ray data suggested a weak C3−H···O interaction with the Gly48 backbone carbonyl group.[10] We therefore envisioned that introduction of a polar substituent at the C3 position may lead to additional interactions of the Cp-THF ligand with the protease flap residues. Furthermore, an inhibitor that makes tight interactions with the protease flap region could conceivably delay its dissociation via opening of the flaps. Herein, we report the design, synthesis, and biological evaluation of a series of protease inhibitors that incorporate a stereochemically defined functionality at the C3 position of the Cp-THF ligand. Inhibitor **26**,

Received: May 20, 2011
Published: July 29, 2011

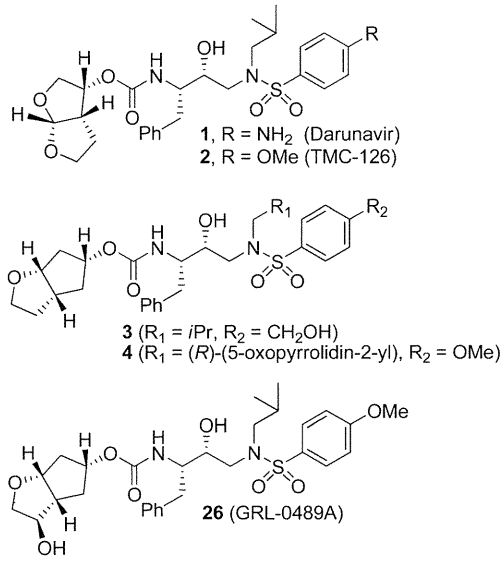

Figure 1. Structures of potent HIV-1 protease inhibitors **1**–**4** and **26**.

Scheme 1. Syntheses of Optically Pure P2 Ligands 7 and 8

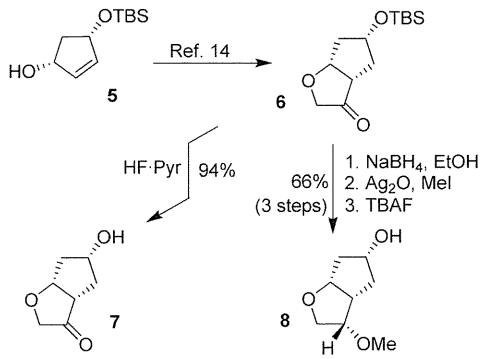

incorporating a 3-(*R*)-hydroxyl group, was the most potent PI (K_i = 5 pM; antiviral IC_{50} = 2.9 nM). This inhibitor also maintained excellent potency against a range of multidrug-resistant HIV-1 variants. The protein–ligand X-ray structure of **26**-bound HIV-1 protease revealed important insights into the ligand-binding site interactions of the inhibitor with the flap region as well as other regions of the HIV-1 protease active site.

CHEMISTRY

The syntheses of 3-keto and 3-(*S*)-methoxy Cp-THF ligands are shown in Scheme 1. Optically active alcohol **5** was prepared in multigram quantities as described previously.[13,14] This was efficiently converted to ketone **6** as reported by us.[14] The removal of TBS ether by exposure to HF–pyridine afforded keto alcohol **7** in 94% yield. Ketone **6** was converted to 3-(*S*)-methoxy derivative **8** in a three-step sequence involving (1) reduction of the ketone with $NaBH_4$ in ethanol at −25 °C to provide the corresponding alcohol as a single diastereomer, (2) methylation of the resulting alcohol with MeI in the presence of Ag_2O in acetonitrile, and (3) removal of the silyl group with TBAF in THF to provide **8** in 66% yield, in three steps.

The syntheses of 3-(*R*)-acetoxy and 3-(*R*)-methoxy ligands **11** and **12** are outlined in Scheme 2. Treatment of alcohol **5** with

Scheme 2. Syntheses of Ligands 11 and 12

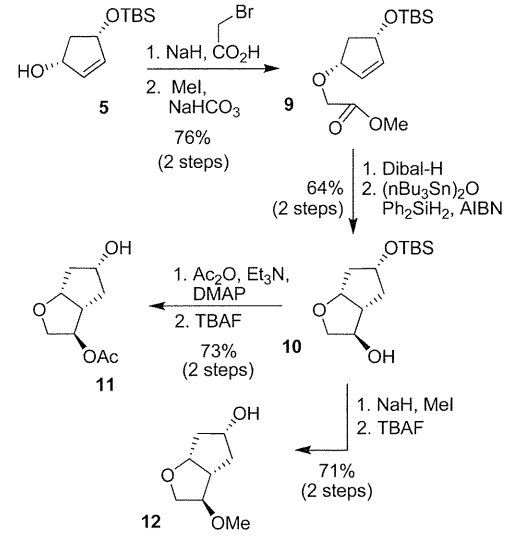

Scheme 3. Syntheses of C3-Methyl-Substituted Ligands 14 and 18

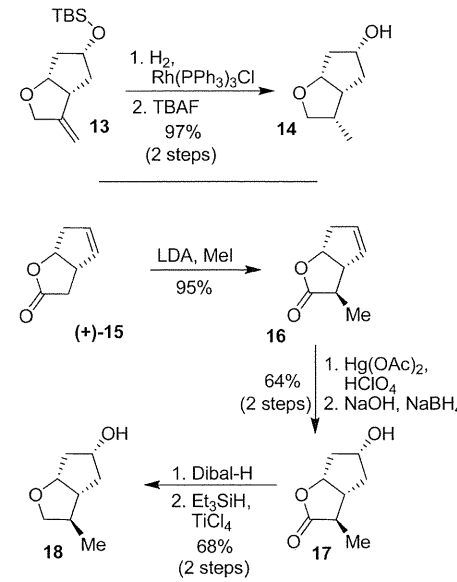

NaH and 2-bromoacetic acid in THF provided the corresponding alkylated acid. The resulting acid was reacted with methyl iodide in the presence of $NaHCO_3$ to provide methyl ester **9** in 76% yield (two steps). DIBAL-H reduction of ester **9** followed by radical cyclization[15] of the resulting alkene using a catalytic amount of $(n\text{-}Bu_3Sn)_2O$, Ph_2SiH_2 and ethanol (2 equiv) in the presence of a catalytic amount of AIBN in benzene provided 3-(*R*)-hydroxy derivative **10** in 64% yield, in two steps. The ^1H NMR results showed a diastereomeric ratio of 10:1. The major isomer was separated by silica gel chromatography and used for the subsequent reactions. Reaction of alcohol **10** with acetic anhydride and triethylamine in the presence of a catalytic amount of DMAP afforded the corresponding acetate. The removal of the silyl group with TBAF in THF provided ligand **11** in 73% yield, in two steps. Alcohol **10** was converted to methoxy derivative **12** by

Scheme 4. Syntheses of Activated Mixed Carbonates 19a–f

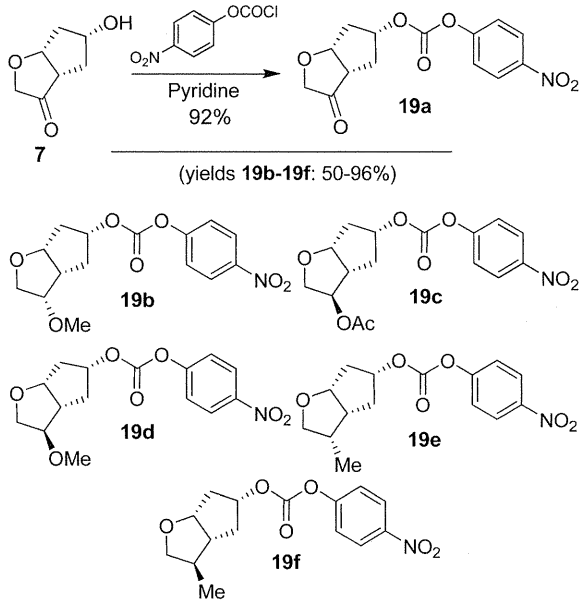

Scheme 5. Syntheses of Inhibitors 21–32

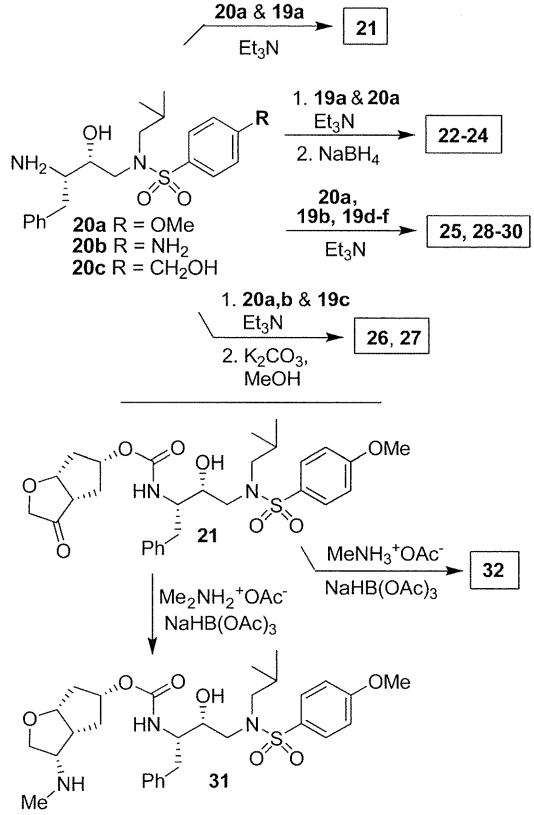

alkylation with NaH and MeI in THF followed by removal of the silyl group in 71% yield (two steps).

We also planned to synthesize stereochemically defined 3-methyl derivatives to compare with the effects of alkoxy and hydroxy groups. Toward this goal, we have carried out stereoselective syntheses of 3-(*S*)- and 3-(*R*)-methyl derivatives, and the synthetic routes are shown in Scheme 3. Optically active olefin **13** was synthesized as described previously.[14] Catalytic hydrogenation of **13** in the presence of Wilkinson's catalyst under a hydrogen filled balloon at 23 °C for 3 h followed by removal of the silyl group using TBAF afforded 3-(*S*)-methyl derivative **14**.[16] For the synthesis of the 3-(*R*)-methyl derivative, commercially available optically active lactone (+)-**15** was methylated using LDA and MeI at −78 °C to provide methyl derivative **16** with high diastereoselectivity (dr = 20:1) and in 95% yield. Olefin **16** was then subjected to oxymercuration condition with $Hg(OAc)_2$ and $HClO_4$. The resulting organomercurial derivative was treated with aqueous sodium hydroxide solution followed by $NaBH_4$ reduction to afford *endo*-alcohol **17** in 64% yield. The lactone was then reduced to the corresponding lactol with DIBAL-H. Further reduction of the resulting lactol using Et_3SiH and $TiCl_4$ furnished 3-(*R*)-methyl derivative **18** in 68% yield. Results from the ^1H NMR NOESY experiments fully corroborated the assignment of 3-(*S*)- and 3-(*R*)-stereochemistry of methyl derivatives **14** and **18**, respectively.

Various optically active ligand alcohols **7**, **8**, **11**, **12**, **14**, and **18** were converted to the respective mixed activated carbonates. As shown in Scheme 4, reactions of ligand alcohols with 4-nitrophenyl chloroformate in the presence of pyridine in CH_2Cl_2 provided activated carbonates **19a–f** in 50–96% yield.[17] The syntheses of designed inhibitors were carried out by coupling these activated carbonates with various hydroxyethylsulfonamide isosteres containing functionalized P2′-phenylsulfonamide ligands. As shown in Scheme 5, amines **20a–c** were readily prepared as described previously.[10,17] Reaction of amine **20a** with carbonate **19a** provided inhibitor **21**. Inhibitors **22–24** were prepared by reaction of carbonate **19a** with respective amines **20a–c** followed by $NaBH_4$ reduction of the resulting ketone derivatives.

The inhibitor structures are shown in Table 1. Inhibitors **25** and **28–30** were prepared by reactions of amine **20a** with mixed carbonates **19b** and **19d–f**, respectively. The synthesis of inhibitors **26** and **27** was carried out by reactions of mixed carbonate **19c** with amines **20a** and **20b** followed by removal of the acetyl group with K_2CO_3 in methanol. All inhibitors were prepared in good to excellent overall (41–96%) yields. The synthesis of inhibitor **31** containing a dimethylamine functionality was carried out by reductive amination of ketone **21** with $Me_2NH_2^+OAc^-$ in the presence of $NaHB(OAc)_3$. We have also attempted to prepare the corresponding methylamine derivative by reductive amination with $MeNH_3^+OAc^-$. However, the resulting 3-(*S*)-methylamine derivative **32** turned out to be unstable.

RESULTS AND DISCUSSION

As mentioned previously, inhibitors were designed to make additional interactions in the S2-subsite of the protease, especially with the Gly48 backbone atoms in the flap region of the enzyme. All inhibitors in Table 1 were first evaluated in enzyme inhibitory assay developed by Toth and Marshall.[18] Inhibitors that exhibited potent K_i were subsequently evaluated for in vitro antiviral assays. As can be seen in the Table 1, all inhibitors displayed subnanomolar to low picomolar inhibitory potencies. Inhibitor **22**, with a 3-(*S*)-hydroxy group on the Cp-THF, was significantly more potent than the keto derivative **21** (entries 1 and 2). The 3-(*S*)-hydroxy Cp-THF ligand was also investigated in combination with other phenylsulfonamide substituents. Inhibitor **23** with a *p*-aminophenylsulfonamide as the P2′-ligand displayed impressive inhibitory potency; however, its antiviral

Table 1. Enzymatic Inhibitory and Antiviral Activity of Inhibitors 21−31

Entry	Inhibitor	K_i (nM)	IC_{50} (nM)[a]	Entry	Inhibitor	K_i (nM)	IC_{50} (nM)[a]
1	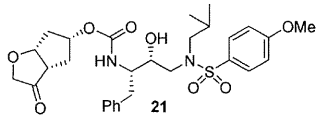 **21**	0.95	14	7	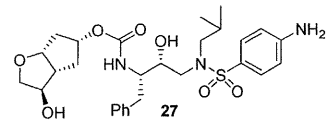 **27**	0.006	36
2	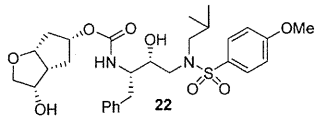 **22**	0.077	7	8	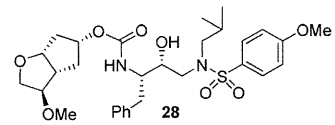 **28**	0.006	3.4
3	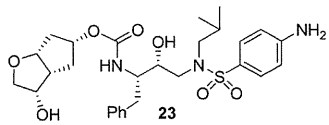 **23**	0.079	25	9	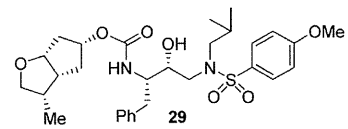 **29**	0.16	25
4	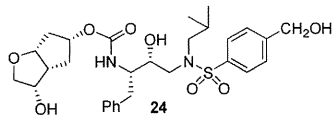 **24**	0.06	19	10	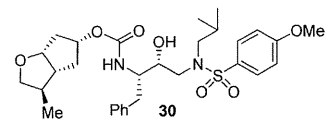 **30**	0.017	---
5	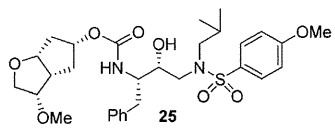 **25**	0.39	37	11	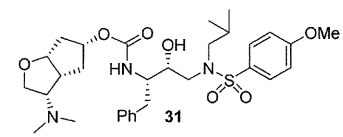 **31**	12.5	---
6	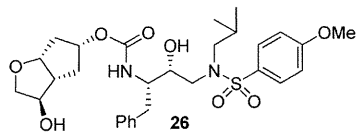 **26**	0.005	2.9				

[a] Values are the mean of at least two experiments. Human T-lymphoid (MT-2) cells (2×10^3) were exposed to 100 $TCID_{50}$ of HIV-1_{LAI} and cultured in the presence of each PI, and IC_{50} values were determined using the MTT assay. The IC_{50} values of amprenavir (APV), saquinavir (SQV), indinavir (IDV), and darunavir (DRV) were 0.03, 0.015, 0.03, and 0.003 μM, respectively.

activity was 3-fold lower than **22**. Inhibitor **24** with a *p*-hydroxymethylphenylsulfonamide as the P2′-ligand has shown a reduction in potency. Inhibitor **25**, which contains a 3-(*S*)-methoxy substituent, exhibited a significant loss of potency and a near 5-fold loss of antiviral activity compared to **22**. Interestingly, inhibitor **26** with 3-(*R*) configuration displayed an impressive enzyme inhibitory and antiviral activity. Inhibitor **27** with the 4-aminophenylsulfonamide isostere also showed comparable enzyme inhibitory activity. Inhibitor **28**, with a 3-(*R*)-methoxy group, also exhibited comparable inhibitory potency.

In order to probe the importance of the C3- oxygen on the Cp-THF ring, inhibitors **29** and **30** with a methyl group in place of a C3-hydroxyl were synthesized. Inhibitor **29**, which contains a 3-(*S*)-methyl group, showed a significant reduction in potency compared to **22**. Similarly, inhibitor **30** with a 3-(*R*)-methyl group has shown a reduction in enzyme K_i compared to the corresponding hydroxy derivative **26**. We have also investigated an amine substitution on the Cp-THF ligand. Inhibitor **31** with C3-dimethylamine exhibited a substantially lower enzyme inhibitory potency compared to the corresponding hydroxy or methoxy derivatives.

Inhibitors **22** with a 3-(*S*)-hydroxyl group and **26** with a 3-(*R*)-hydroxyl group on the Cp-THF ligand were tested against a panel of multidrug-resistant HIV-1 variants. Their antiviral activity was compared against other clinically available PIs including APV and DRV. The results are shown in Table 2. All inhibitors in Table 2 exhibited high antiviral activity against the wild-type HIV-1 laboratory strain, HIV-$1_{ERS104pre}$, isolated from a drug-naive patient.[7] Compound **26** provided the most potent activity with an IC_{50} of 2.9 nM, comparable to that of DRV. When tested against various multidrug-resistant HIV-1 strains, the IC_{50} of inhibitor **26** remained in the low nanomolar range (2.9−29 nM) and fold-change in IC_{50} did not exceed 10. Interestingly, isomeric inhibitor **22** displayed lower activity against the wild-type viral strain (IC_{50} = 20 nM). It also exhibited a much larger IC_{50} fold change and in some cases only marginal activity against multidrug-resistant HIV-1 variants. Such a stark contrast in antiviral activity of **22** compared to **26** emphasizes the importance of the stereochemistry at the C3-position of the Cp-THF ligand. Inhibitor **26** displayed a superior profile compared to another approved PI, APV. Overall, inhibitor **26** maintained impressive potency against all tested multidrug-resistant HIV-1 strains. It compared favorably with DRV, which is the leading PI for the treatment of multidrug resistant HIV infection.

In order to gain molecular insight into the ligand/binding-site interactions responsible for the activity of inhibitor **26**, we have determined the X-ray crystal structure of the inhibitor-bound wild-type HIV-1 protease that was refined to a 1.45 Å resolution. The protease dimer binds with the inhibitor in two orientations

Table 2. Comparison of the Antiviral Activity of 22, 26, and Other PIs against Multidrug Resistant HIV-1 Variants

	$IC_{50} \pm SD$, μM (fold change)[b]			
virus[a]	APV	DRV	22	26
HIV-$1_{ERS104pre}$(wt)	0.030 ± 0.006	0.0037 ± 0.0001	0.020 ± 0.004	0.0029 ± 0.0008
HIV-$1_{MDR/B}$	0.93 ± 0.28 (31)	0.036 ± 0.013 (10)	>1 (>50)	0.029 ± 0.007 (10)
HIV-$1_{MDR/C}$	0.26 ± 0.03 (9)	0.013 ± 0.0004 (4)	>1 (>50)	0.022 ± 0.003 (7)
HIV-$1_{MDR/G}$	0.38 ± 0.03 (12)	0.0023 ± 0.0006 (1)	0.27 ± 0.02 (13)	0.0045 ± 0.0007 (2)
HIV-$1_{MDR/TM}$	0.19 ± 0.06 (6)	0.0019 ± 0.0003 (1)	0.041 ± 0.004 (2)	0.0031 ± 0.002 (1)

[a] Amino acid substitutions identified in the protease-encoding region compared to the consensus type B sequence cited from the Los Alamos database: L10I, L33I, M36I, M46I, F53L, K55R, I62 V, L63P, A71 V, G73S, V82A, L90M, and I93L in HIV-1MDR/B; L10I, I15 V, K20R, L24I, M36I, M46L, I54 V, I62 V, L63P, K70Q, V82A, and L89 M in HIV-1MDR/C; L10I, V11I, T12E, I15 V, L19I, R41K, M46L, L63P, A71T, V82A, and L90 M in HIV-1MDR/G; L10I, K14R, R41K, M46L, I54V, L63P, A71V, V82A, L90M, I93L in HIV-$1_{MDR/TM}$. HIV-$1_{ERS104pre}$ served as a source of wild-type HIV-1. [b] IC_{50} values were determined by using PHA-PBMs as target cells, and inhibition of p24 Gag protein production by each drug was used as an end point. Numbers in parentheses represent *n*-fold changes of IC_{50} for each isolate compared to IC_{50} for the wild-type HIV-$1_{ERS104pre}$. All assays were conducted in duplicate or triplicate, and data shown represent mean values (±1 standard deviation) derived from results of three independent experiments. PHA-PBMs were derived from a single donor in each independent experiment. DRV: darunavir. APV: amprenavir.

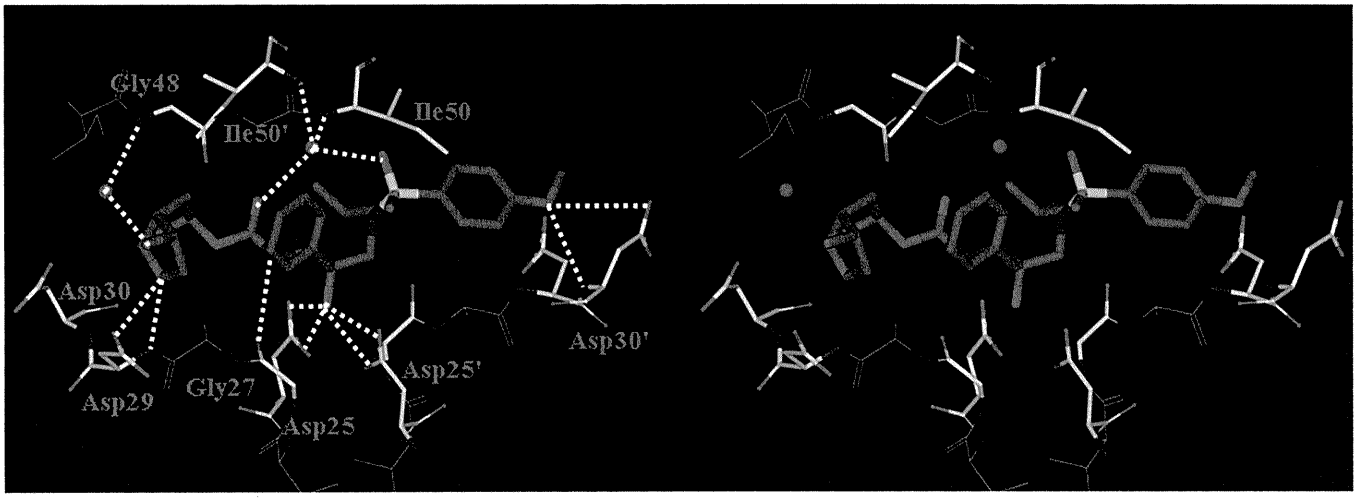

Figure 2. Stereoview of the X-ray structure of inhibitor **26** bound to the active site of the wild-type HIV-1 protease.

related by a 180° rotation with a 0.55/0.45 ratio. The protease backbone structure showed a very low rms deviation of 0.15 Å for all Cα atoms compared to protease complexes of **2** or darunavir.[19,20] The inhibitor makes extensive interactions from the P2 to P2′ ligands with the protease atoms and most notably displays favorable polar interactions including hydrogen bonds, weaker C−H···O and C−H···π interactions, as shown in Figure 2. The central hydroxyl group forms hydrogen bonds with the side chain carboxylate oxygen atoms of the catalytic Asp25 and Asp25′ residues. The inhibitor hydrogen-bonds with the protease backbone atoms of the amide of Asp30′, the carbonyl oxygen of Gly27, and forms water-mediated interactions with the amides of Ile50 and Ile50′, which are generally conserved in the majority of protease complexes with inhibitors[21] or substrate analogues.[22,23] The inhibitor interactions with atoms in the binding cavity resemble those of darunavir and **2** (TMC-126) with the exception of the interactions of the new P2-ligand that replaces the bis-THF group. The 3-(*R*)-hydroxyl of the Cp-THF ligand extends toward the flap region and forms a new water-mediated hydrogen bond interaction with the backbone amide NH of Gly48, with interatomic distances of 2.5 and 3.1 Å for the major inhibitor orientation or 2.7 and 3.1 Å for the minor orientation. Also, the Cp-THF ether oxygen forms a strong hydrogen bond with the backbone amide NH of Asp29. These new interactions with the backbone atoms of Gly48 are likely to be responsible for the impressive antiviral activity and drug resistance properties of this inhibitor. The C3-functionality on the Cp-THF appears to enhance the affinity of the inhibitor. The new water-mediated interaction with the backbone NH of Gly48 on the protease flap may promote thermodynamic stabilization of the closed conformation of the protease−ligand complex. This may slow the kinetics of dissociation of the inhibitor through flexible opening of the protease flap.

■ CONCLUSION

In summary, we have designed a number of C3-substituted hexahydrocyclopentafuranylurethanes as P2-ligands to enhance interactions with the protein backbone in the S2-subsite. The ligands were stereoselectively synthesized in optically active form. Incorporation of these ligands in (*R*)-hydroxyethylsulfonamide isosteres resulted in a series of novel and highly potent HIV-1 protease inhibitors. In particular, inhibitor **26** displayed remarkable enzyme inhibitory and antiviral potency. Also, inhibitor **26** has shown excellent activity against multi-PI-resistant